PennWell®
www.laserfocusworld.com
March 2016

Laser Focus World®

Photonics Technologies & Solutions for Technical Professionals Worldwide

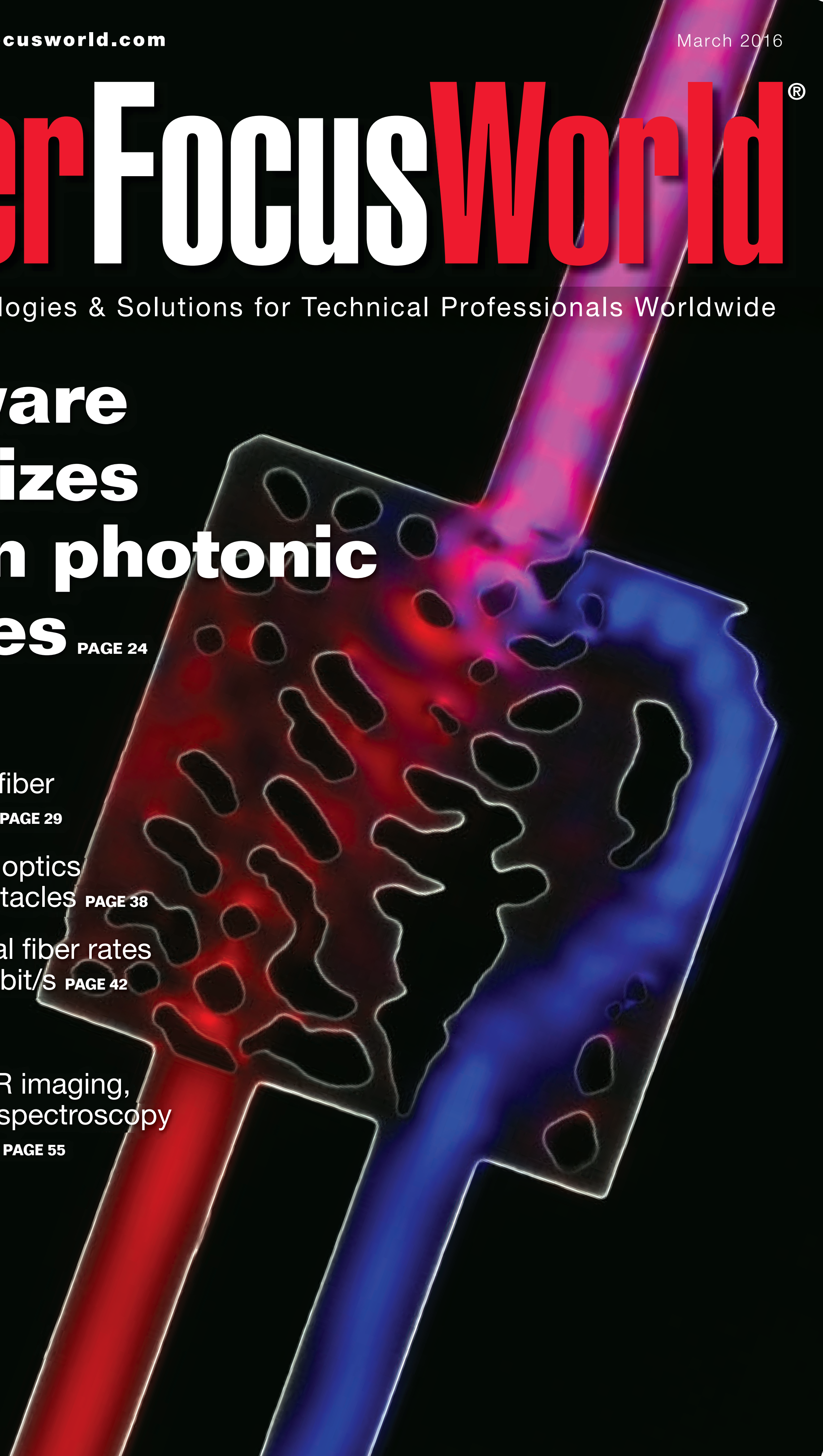

Software optimizes silicon photonic devices PAGE 24

- Kilowatt-level fiber lasers mature PAGE 29
- Ultrafast laser optics overcome obstacles PAGE 38
- Pushing optical fiber rates beyond 100 Gbit/s PAGE 42

BioOptics World®

- Deep brain NIR imaging, SWIR Raman spectroscopy for melanoma PAGE 55

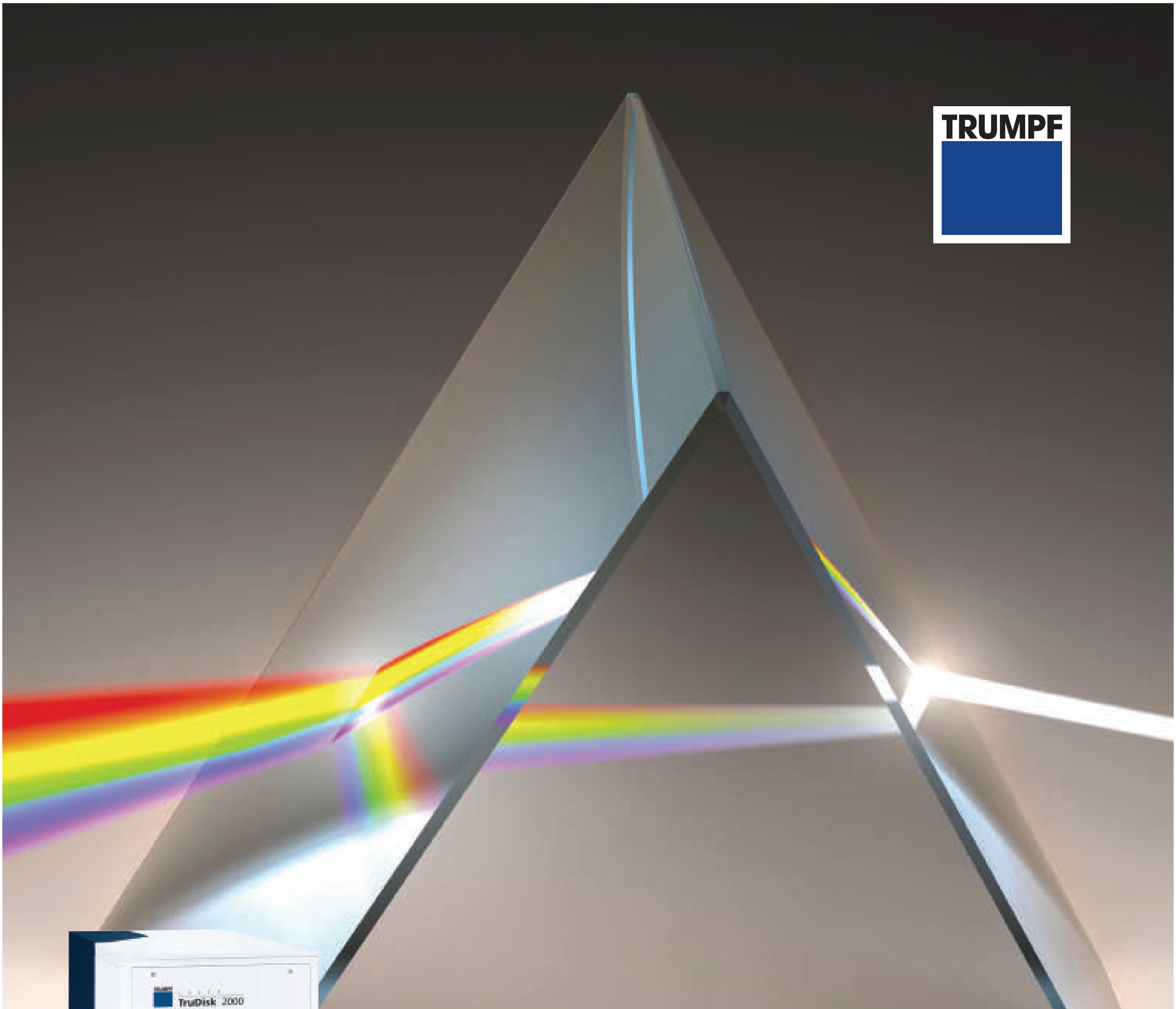


TruDisk 2000

LaserFocusWorld®
Photonics Technologies & Solutions for Technical Professionals Worldwide

MARCH 2016 ▪ VOL. 52, NO. 3

newsbreaks

world news

columns

departments

LASERS ▪ OPTICS ▪ DETECTORS ▪ IMAGING ▪ FIBER OPTICS ▪ INSTRUMENTATION

features

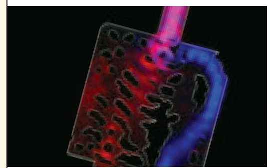

24 COVER STORY
An electron micrograph of a compact demultiplexer device is overlaid with simulated electromagnetic fields at 1300 nm (blue) and 1550 nm (red). *(From A. Y. Piggott et al.,* Nature Photon.*, 9, 6, 374–377 [2015], with permission)*

LASER FOCUS WORLD PRESENTS
BioOptics WORLD

Coming in April

Next month includes special articles to highlight what's hot in many important areas:
- Contributing editor Jeff Hecht continues his Photonic Frontiers series by discussing high-efficiency optical pumping.
- Articles on high-speed cameras, infrared optics, extreme light from very high-energy lasers, precision molded aspheres, and diamond anvils and their optical uses.

In *BioOptics World*, we will have articles on optical microscopy for bioanalysis and optical coherent microscopy.

cool content

Blog: Photon Focus

Senior editor John Wallace provides some analysis and commentary on China's strong presence in photonics. Keep coming back to our blog for more hot topics, cool commentary, and other events-related musings!
http://bit.ly/14RIfUO

Technical Digests dig into technology topics

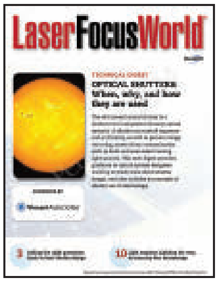

Laser Focus World offers free downloadable technical digests that provide an in-depth resource on photonics and optoelectronics topics, including **optical shutters** and **photoluminescence**.
http://bit.ly/ViD38v

Webcasts let you make new discoveries from your desktop

Whether you are looking to learn about **understanding ultrafast scientific lasers**, **specialty optical fibers**, or **wave optics simulations**, we've got webcasts aplenty to meet your educational needs.
http://bit.ly/Onhs9J

White papers offer detailed tech specs on many products

Our library of technical white papers delves into performance attributes of several optics and photonics products available on the market, including an **ultrafast optical sampling oscilloscope** and **wire-grid polarizing beamsplitters**.
http://bit.ly/1BUCpTf

www.laserfocusworld.com

trending now

Focus on Lasers & Sources
Laser Focus World *covers the design and applications of all types of lasers, amplifiers, and other advanced sources like light-emitting diodes (LEDs). Here are three of our most popular articles on this topic.*

LEDs are workhorses with applications far beyond lighting

Deep-UV LEDs could power new water-quality monitoring networks, near-UV LEDs cure adhesives and inks, micro-LEDs open doors for optogenetic research, and direct-bandgap GeSn LEDs can be fabricated on silicon.
http://bit.ly/1XKLSaB

Laser diode operation 101: A user's guide

As laser technology proliferates, end users are coming into contact with lasers for the first time, and are unfamiliar with the unique and unintuitive requirements of operating a laser safely, effectively, and consistently.

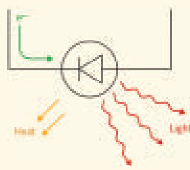

http://bit.ly/1plEc2Q

Green thin-disk laser emits 400 W CW in a near-fundamental mode

Scientists in Germany have created a continuous-wave (CW) thin-disk laser that uses intracavity second-harmonic generation to reach an output power of 403 W at a 515 nm wavelength with an almost diffraction-limited beam.

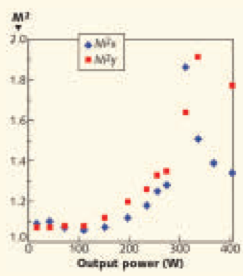

http://bit.ly/1QH5re0

Knowing what's behind the curtain

Fiber-optic communications technology is so intrinsic to our Internet-enabled, cloud-driven, instant-video world that it has become essentially invisible to most people—a bit like the Wizard of Oz in the 1939 movie, who hides behind a curtain while performing all sorts of magic tricks for Dorothy and her companions Scarecrow, Tin Man, and Cowardly Lion. When I try to explain in the simplest terms how the magic works to non-technical friends and family, the extent of response is along the lines of, "so that's how the cat video gets on my Facebook page."

Fortunately, the engineers engaged in developing the next generation of optical communications know very well what's behind the curtain. That is clearly the case this month in our OSA Future Optics interview with Neal Bergano, vice president and CTO at TE Connectivity SubCom, who has spent his professional life helping to develop and deploy the undersea fiber-optic network that encircles the globe (see page 21). It's also evident in our Photonic Frontiers article from contributing editor Jeff Hecht, who describes the research efforts underway to extend optical fiber transmission rates beyond 100 Gbit/s (see page 42). And the same applies to the researchers of future products at the Ginzton Laboratory of Stanford University, whose article on designing silicon photonic devices provides the cover story for this issue (see page 24). Much more on these topics can be learned at the Optical Fiber Communications (OFC) Conference and Exhibition, March 20-24, in Anaheim, CA.

The Internet is not the only magic that optical fiber communications has wrought, of course. Senior editor John Wallace's article reviewing the currently available lineup of kilowatt-class fiber lasers shows that a technology first deployed for the amplification of undersea optical communications has been successfully adapted to a very dissimilar application, materials processing (see page 29).

The curtain around such engineering wizardry is not such a bad thing, as long as we know how to keep building those magical levers and switches.

Conard Holton
Associate Publisher/ Editor in Chief
cholton@pennwell.com

newsbreaks

Single-photoelectron calibration of PMTs needs no analytical model

Photomultiplier tubes (PMTs) are essential components of many scientific and other optical systems that are designed to measure very low light levels. For optimal calibration, PMTs are important. Often, a PMT is not being used to count photons singly, but is instead measuring slightly higher levels where the photon signals overlap. However, the PMT must provide an accurate estimate of the photon rate and the relative width of the single photoelectron pulse. In this case, the PMT is conventionally calibrated relative to the mean of the charge distribution that corresponds to the single photoelectron (SPE) produced by a single detected photon. This is done using a very low-intensity light source and an analytical model of the SPE response, but defining that analytical model is extremely difficult because of the complexity of the process.

Researchers at the University of Chicago (Chicago, IL) and the Fermi National Accelerator Laboratory (Batavia, IL) have come up with a way to extract the relevant SPE calibration parameters using simple statistics and no assumption about the SPE distribution. To ensure the correct statistical estimate, the approach includes the underamplified component of the SPE response in the estimate of the mean and variance. The researchers experimentally verified the effectiveness of the new method by calibrating a Hamamatsu R11410 PMT, as well as Monte Carlo simulations. Their approach produced accurate estimates of the SPE mean and variance to better than 5% and 6%, respectively, at PMT gain values above 1×10^7. The researchers say that the method is effective over a wide range of intensities, thus allowing calibration of arrays of PMTs that receive nonuniform illumination because of their large size. *Reference: R. Saldhana et al.*, arXiv:1602.03150v1 [physics.ins-det] *(Feb. 9, 2016).*

Experimental setup

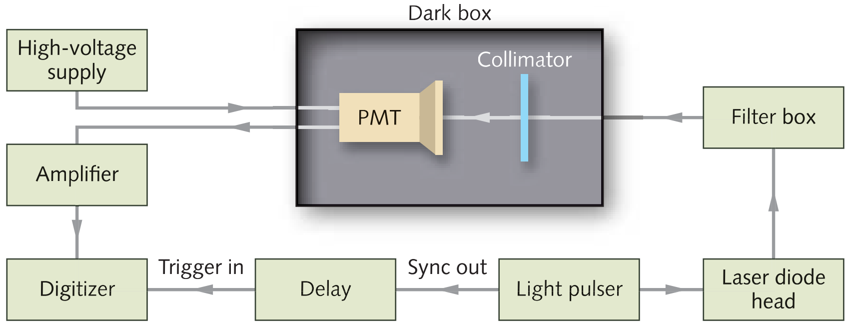

Structured-light projector for bicyclists has green diode laser

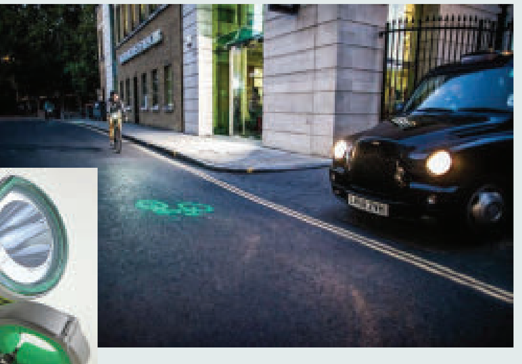

Recognizing that the safety of bicyclists is dependent on their ability to be seen by other motorists, Emily Brooke, founder and CEO of BLAZE (London, England), developed the BLAZE Laserlight bike light that projects a bright-green image of a bicycle 6 m ahead on the pavement. The laser projection system within BLAZE not only provides a bright-white LED for up to 300 lumens of general illumination for the cyclist, but also includes a 520-nm-wavelength green laser diode with a 30 mW power output that projects the image while consuming 2900 mA of electrical power from its battery.

To project this structured-light image that far while maintaining high intensity, the BLAZE Laserlight takes advantage of an eye-safe, low-divergence, high-brightness green laser and diffractive optics. Both the LED and laser can be operated in continuous or flashing mode, with the battery providing two hours of operation when both the laser and the LED headlight are at maximum continuous power, and up to 29 hours of operation when the LED is at 100 lumens and the laser is off. The unit is manufactured by the same company that makes Apple products and is commercially available for less than $180. *Reference: https://blaze.cc/laserlight.*

Polarization switching improves laser guide star brightness

An artificial laser guide star (LGS) generated by illuminating the mesosphere at 90 km altitude with a 589 nm laser to excite a sodium atom layer is a critical process for astronomical adaptive optics (AO) applications. The artificial beacon, placed in the vicinity of an astronomical object being studied, is subject to similar atmospheric perturbations and offers a route to AO-based image correction. Because improved LGS brightness improves AO outcomes, researchers are using such brightness-boosting techniques as circular polarization, pulsing the laser at the Larmor frequency to mitigate geomagnetic field effects, or, in a simpler method developed by researchers at the Shanghai Institute of Optics and Fine Mechanics (SIOM; Shanghai, China) and the University of the Chinese Academy of Sciences (Beijing, China), polarization switching.

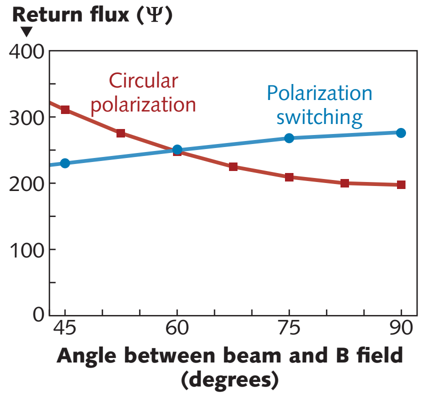

By using a commercially available electro-optic phase modulator and aligning the polarization of the laser at a 45° angle with the optical axis of the electro-optic crystal, applying voltage to the crystal can produce a variable phase delay that alternates between $-\pi/2$ and $+\pi/2$, switching the laser between left and right circular polarization at the Larmor frequency on the order of 100 kHz. This "magnetically resonant pumping" method uses an optics module that can be retrofitted to any existing or future continuous-wave (CW) LGS laser and can increase return flux at most astronomical observation angles (around 60° to 90°) by as much as 50%. *Reference: T. Fan et al.,* Sci. Rep., *6, 19859 (Jan. 22, 2016).*

Nanoplasmonic device efficiently converts IR to green light

Research conducted at the University of Alberta (Edmonton, AB, Canada) has resulted in the successful demonstration of the generation of green light from a silicon-on-insulator (SOI) nanoplasmonic waveguide using third-harmonic generation (THG). This THG device is excited at its input by a 1550 nm laser input that is guided by a silicon waveguide 340 nm high and 95 nm wide with a 60-nm-thick layer of gold (Au) fabricated on a silicon-on-insulator (SOI) substrate, resulting in green emission at 517 nm at the output face.

Understanding that silicon (Si) has the highest third-order nonlinear coefficient of all CMOS materials and the highest refractive index, visible light emission is normally difficult because of the indirect Si bandgap and strong absorption of any visible light that is generated. To combat these obstacles, the waveguide takes advantage of strong light-matter coupling from the surface-plasmon mode in the waveguide and strong confinement of the infrared electric field to enable efficient nonlinear optical mixing and THG over a short distance that is less than the absorption length of green light in Si (about 700 nm). The waveguide can also generate broadband visible light by ponderomotively accelerating the photoexcited electrons in the steep field gradient at the Si-Au interface and driving an electron avalanche multiplication and impact-ionization processes in the strong nanoplasmonic field. *Reference: S. Sederberg and A. Y. Elezzabi,* Phys. Rev. Lett., *114, 22, 227401 (Dec. 2015).*

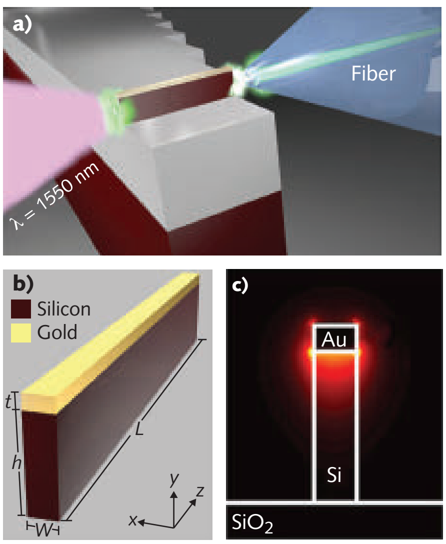

world news

Frequency comb

See page 14

Technical advances from around the globe

Got News? Please send articles to johnw@pennwell.com

ATTOSECOND TECHNOLOGY

Visible-light pulses are only 380 attoseconds long

Scientists have for years been doing productive research using ultrafast light pulses with durations down to 2 or 3 fs. Now, researchers at the Max Planck Institute for Quantum Optics and Ludwig-Maximilians University (both in Garching, Germany), Texas A&M University (College Station, TX), and M.V. Lomonosov Moscow State University (Moscow, Russia) have pushed visible-light pulses beyond the femtosecond region into the attosecond (as) regime, creating pulses in the visible-light region only 380 as long.[1] The group is headed by Eleftherios Goulielmakis, who is already well-known for his research into attosecond technology and science.

The new technique is in contrast to the more-usual production of attosecond pulses using high-harmonic generation (HHG), in which light is created over a very broad spectrum into the x-ray region, with the wide spectrum allowing the production of pulses under 100 as in duration (Goulielmakis and his lab are leaders in this area, too).

The optical attosecond pulses will enable not only science, as they for the first time provide direct access to the nonlinear response of bound electrons; they may also lead to photonic devices operating at subfemtosecond time scales and at petahertz (10^{15} Hz) rates.

Light-field synthesizer

The group created optical attosecond pulses using a light-field synthesizer that can manipulate the properties of visible light along with nearby infrared (IR) and ultraviolet (UV) frequencies—about 1.1 to 4.6 eV, or on the order of 1130 to 270 nm. The synthesizer managed broadband and almost dispersion-free spectral equalization of the synthesized pulses, producing pulses with twice the initial bandwidth. The resulting 380 as light pulses are so short that they are barely more than a half-oscillation of a light field in duration, making them the fastest pulses of visible light ever created.

First, broadband (1.1–4.6 eV) light pulses are generated via nonlinear broadening of laser pulses with 22 fs duration, 1 mJ energy, and 790 nm wavelength achieved by passing them through a hollow-core fiber filled with neon gas; the supercontinuum pulses have energies of about 550 μJ each.

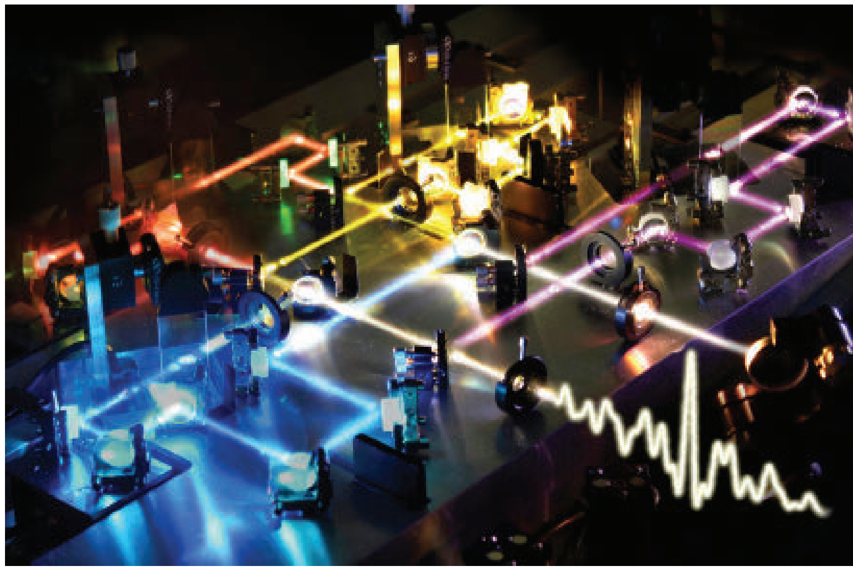

To create an attosecond optical pulse, a few-femtosecond continuum pulse is spectrally divided into four bands (represented here by colors), each of which is separately compressed using dispersive mirrors. The four pulses are then combined precisely in space and time to produce the final pulse (represented here by white, with the half-cycle temporal pulse shape shown at bottom right). *(Courtesy of Eleftherios Goulielmakis)*

Each of these pulses is then spectrally divided into four spectral bands: near-infrared (NIR; 1130–710 nm), visible (710–500 nm), visible-UV (500–350 nm), and deep-UV (350–270 nm). Each of the four resulting pulses is individually compressed via dispersive mirrors to durations of 8.5 fs for the NIR pulse, 7 fs for the visible, 6.5 fs for the visible-UV, and 6.5 fs for the deep-UV pulse. The four pulses are then recombined spatially and temporally to create the final attosecond pulse, which has an energy of about 320 μJ (see figure).

The physical overlaying of the four spectrally divided pulses to create the attosecond pulse must be done very precisely. In addition, the intensity of each of the four pulses is carefully controlled to achieve the proper spectral-band power in relation to the other three pulses. To produce longer, single-cycle pulses, the short-wavelength (<410 nm) end of the attosecond half-cycle optical pulse's spectrum can be optically removed—the resulting narrower spectrum leads to a longer pulse.

Resulting science

The researchers focused optical attosecond pulses onto a cell filled with krypton gas at a pressure of 80 mbar, generating vacuum-UV (VUV) spectra. A spectrometer placed downstream from the cell probed the resulting nonlinear polarization. The measured spectra ranged from 5 to 14 eV (250 to 89 nm)—this was possible because the sampled spectra do not overlap at all with the spectrum of the optical attosecond pulses. The results showed a finite nonlinear response time of bound electrons of up to 115 as, controllable via the field of the optical attosecond pulses.

The researchers say that it should be possible to extend the technique to the analysis of solids as well, with the potential to push the limits of optical signal processing by achieving ever-faster rates.—*John Wallace*

REFERENCE

1. M. Th. Hassan et al., *Nature*, doi:10.1038/nature16528 (Feb. 3, 2016).

FREQUENCY COMBS

FOKUS frequency comb launches into space again, compares three clock frequencies

The Faserlaserbasierter Optischer Kammgenerator unter Schwerelosigkeit (FOKUS) instrument from Menlo Systems (Martinsried, Germany) traveled into space on January 23, 2016, aboard the German Space Agencies' (DLR) TEXUS 53 sounding rocket for a second time since the April 2015 inaugural launch of a similar Menlo frequency comb.

Building on the 2015 success in operating a frequency comb in space, this 2016 launch allowed six minutes of experimental time to conduct a comparison of three clock frequencies: two optical clocks using

rubidium and potassium atoms, and one radio-frequency (RF) clock based on rubidium atoms.

In addition to measuring optical frequencies with the accuracy of RF atomic clocks, optical frequency combs are also used for ultralow-noise microwave generation, laser frequency referencing of lidar instruments, and high-speed and high-resolution molecular spectroscopy.

FOKUS' anatomy

The upper part of FOKUS contains the analog and digital control electronics, while the lower part includes three optics modules: the pump laser module with pump diodes for the frequency-comb oscillator and optical amplifiers; the frequency-comb module with laser oscillator, optical amplifiers, a nonlinear interferometer for phase stabilization, and beat-detection units for 780 nm; and the 780 nm distributed-feedback (DFB) laser and its saturation-spectroscopy module (see figure).

Thanks to careful engineering, the FOKUS optical frequency-comb module has been launched into space for a second time, performing without error and setting an important precedent for future research. *(Courtesy of Menlo Systems)*

For the recent launch, an additional amplifier, second-harmonic stage, and mixing optics for beat detection of 767 nm light were added, as well as a more sophisticated 10 MHz reference based on a rubidium clock.

The Menlo optical frequency comb uses a 1.5 μm fiber-laser source and an all-optical-fiber design with telecommunications-grade components. All fibers, couplers, and isolators are polarization-maintaining and embedded in space-proof silicon for improved thermal and mechanical stability. In addition to its femtosecond mode-locked laser source, the comb module includes an erbium-doped fiber amplifier (EDFA) and nonlinear interferometer for carrier-envelope-offset detection, a second-harmonic-generation (SHG) stage, and mixing/filtering optics for 780 nm rubidium and 767 nm potassium laser light.

The rubidium laser module from Humboldt University of Berlin and the Ferdinand Braun Institute comprises a DFB laser and a Doppler-free rubidium spectroscopy module. This miniature spectroscopy module for laser frequency stabilization includes Zerodur-based beamsplitters, mirrors, waveplates, fiber-coupling lenses, a rubidium vapor cell, an electro-optical modulator, and the photodiodes needed to detect a saturation spectroscopy signal and to derive an error signal for frequency stabilization.

A separate potassium stabilized laser module (KALEXUS) was situated on the same TEXUS payload and optically interconnected with FOKUS for the clock comparison.

Frequency comb operation

Essentially a mode-locked laser emitting short optical pulses, the frequency comb has two degrees of freedom: the laser repetition rate and the carrier envelope offset. Offering a train of optical pulses spaced by the inverse repetition rate (10 ns for FOKUS), the individual lines have a well-defined mode distance of 100 MHz.

The comb is phase-stabilized and referenced to a rubidium atomic clock with a 10 MHz clock output. Therefore, the FOKUS optical frequency comb module links the RF domain (kilohertz to a few gigahertz) with the optical domain (hundreds of terahertz). Continuous-wave (CW) laser light from the rubidium- or potassium-stabilized laser are combined with the comb spectrum in the beat-detection units, where the frequency difference between the CW laser line and the next tooth of the comb is detected in a heterodyne beating measurement.

During launch and landing, the comb had to withstand vibrations up to 8 g root-mean-squared (RMS), 15 g shock levels, and constant accelerations up to 13 g while remaining operational. During the micro-g phase, it was automatically brought to a fully phase-locked state and successfully conducted the clock comparison. Its comparison of the three clocks still needs to be evaluated in detail, but is expected to agree with the local position invariance (LPI) to a level of 10^{-1} to 10^{-2}.

The clock comparisons are a prototype experiment for future satellite-based tests meant to study fundamental physics—specifically, testing Einstein's general theory of relativity (namely the LPI) saying that gravity has the same influence on all clocks, no matter how they are constructed. This successful flight shows the technological maturity of the frequency comb and demonstrates its readiness for operation outside of the metrology lab.—*Gail Overton*

REFERENCE

1. See http://bit.ly/1LEEgiV, from Menlo Systems' website (www.menlosystems.com).

INTEGRATED PHOTONICS

Fin optical waveguide will aid co-integration of photonics with electronics

The ability of an integrated-photonics optical waveguide to confine light is ordinarily created by building the waveguide atop a continuous layer of low-refractive-index material, allowing the waveguide to channel light via total internal reflection. For example, in silicon photonics, a continuous layer of silicon dioxide (SiO_2) is ordinarily placed underneath the network of silicon waveguides to allow them to function.

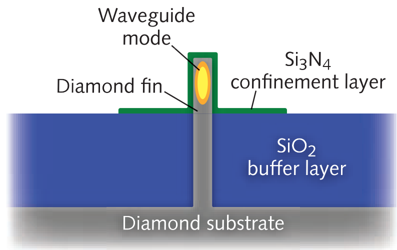

An example of a fin waveguide in diamond-based integrated photonics shows the physical connection of the light-carrying portion of the diamond waveguide with the diamond substrate. The waveguide by itself in air would be too thin to carry the fundamental mode, but with the addition of a silicon nitride (Si_3N_4) confinement layer to its upper portion, the upper part of the waveguide can channel light. A low-index SiO_2 buffer layer spanning most of the lower portion of the waveguide supports the waveguide, but eliminates any light-carrying modes in the lower portion.

However, in silicon photonics, the fact that the low-index layer is continuous creates problems for the integration of photonics with electronics. In other types of integrated photonics, such as those based on III-V semiconductors, silicon carbide (SiC), or diamond, the required buried layer of low-index material weakens the structure and complicates fabrication.

To solve this problem, Richard Grote and Lee Bassett, researchers at the Quantum Engineering Laboratory, Department of Electrical and Systems Engineering, University of Pennsylvania (Philadelphia, PA), have come up with a waveguide geometry that simultaneously allows confinement of light and a physical connection with the substrate of the same material (see figure).[1]

The fin is spanned by a low-index material in its lower portion and a higher-index material at its top, creating an effective index high enough to carry light at the top, but not in the lower portions. And the all-important physical connection to the substrate is maintained.

CMOS-compatible

For silicon photonics, the structure works with CMOS-compatible co-integration of the silicon photonic components with very large-scale integration (VLSI) electronics, such as those used in computer chips. For other types of integrated photonics, the arrangement provides strength and simplicity.

In one example, a diamond fin and substrate with a refractive index of about 2.4 and operating at a 637 nm wavelength are surrounded by a thick SiO_2 buffer layer with an index of 1.45 and a thin (200 nm) silicon nitride (Si_3N_4) confinement layer with an index of 2.0 (see figure). Even though the refractive indices of both SiO_2 and Si_3N_4 are below that of diamond, the fin still confines light. The reason is that the combination of indices in different regions creates differing effective indices, which are high enough for confinement in the Si_3N_4-affected region, but not in the SiO_2 region.

If the waveguide fin itself is too narrow, it cannot carry the lowest-order mode; if it is too wide, light leaks out the bottom and down the fin into the substrate. If the confinement layer is too broad along the fin, a higher-order mode results. Proper confinement and propagation via the fundamental mode depends on a balance of geometry and effective indices. The resulting propagation loss because of substrate leakage is <0.15 dB/cm.

High-*Q* microring resonator

A circular fin waveguide can be used to create a microring resonator. For example, the bending loss for a diamond fin curved to a radius of 10 μm is <0.06 dB per 90° bend using a buffer layer thickness of 2.5 μm. This allows a 20-μm-diameter microring resonator to be made that has an unloaded quality factor Q >30,000.

In another example, a silicon waveguide fin with a SiO_2/Si_3N_4 buffer/confinement structure is designed for single-mode propagation at the telecommunications wavelength of 1.55 μm. In this case, loss because of substrate leakage is calculated to be <1.0 dB/cm, and a 20-μm-diameter microring resonator of silicon would have a Q >10,000.

The researchers note that using the fin waveguide design in indium phosphide (InP)-based photonic integrated circuits would provide an alternative to the conventional indium gallium arsenide (InGaAs) guiding layer, resulting in higher confinement and a smaller mode area.— *John Wallace*

REFERENCE

1. R. R. Grote and L. C. Bassett, *arXiv:1601.01239v1 [physics.optics]* (Jan. 6, 2016).

Undersea fiber optics connect the world today and tomorrow

OSA: *What is the role of submarine fiber optics?*

Neal Bergano: Undersea fiber-optic cables enable a connected world and make the Web worldwide. We may think of the Internet as an abstract thing, but the Internet is built on the physical layer of fiber optics and high-speed integrated circuits.

OSA: *How did you get involved?*

NB: Peter Runge and Dave Ross hired me in 1981 at Bell Labs into a group developing fiber optics as the next technology for transoceanic cables. The state-of-the-art then was analog coaxial cable, which could carry a few thousand 3 kHz voice circuits, but could not scale further. We had a lot to learn. We didn't know if low-loss fibers could be made strong enough to withstand the strain of a cable being laid on the sea bottom and being recovered for repairs.

Undersea fiber cables became a huge paradigm shift. The first transatlantic fiber cable, TAT-8, had only about a factor of five more capacity than the last coaxial cable, but digital fiber transmission enormously improved the quality of a phone call. Overseas calls on analog coaxial cables were noisy and could have echoes. Satellite calls were delayed.

I knew what to expect, but I was still surprised by how good my first call over TAT-8 sounded. A guy I was working with called me from Britain the night before Isaac Asimov made the "first call" on the system, and said "no matter what you hear on television tomorrow, these are the first calls going over the cable."

NEAL BERGANO is vice president and chief technology officer at TE Connectivity SubCom, which has supplied well over 500,000 km of submarine fiber-optic cable. Trained in electrical engineering and optics, he joined the Bell Labs group developing the first transoceanic fiber-optic cable in 1981, and spent his entire career on submarine optical systems. He is a fellow of IEEE, OSA, AT&T, and TE Connectivity, and the recipient of the 2002 John Tyndall Award.

OSA: *How did capacity increase?*

NB: Those first digital fiber systems were hybrid systems with electro-optical repeaters. The repeater converted the high-speed optical signal into electrical form and processed it in integrated circuits to drive a laser transmitter. That bottleneck limited fiber capacity.

The paradigm shift that expanded capacity was the erbium-doped fiber amplifier. I got in on the ground floor by setting up a lab to play with amplifiers in the late 1980s. We had a huge chicken-and-egg problem. You could never build a full-length transmission experiment without a huge development program, but you needed a validation experiment to justify a development program. That led us to invent the circulating loop testbed. We concatenated fibers and optical amplifiers to make a modest amplifier chain, and sent signals through that 120 km loop again and again to emulate transoceanic transmission. We discovered all kinds of interesting things with that system.

We tried to demonstrate transoceanic transmission of a 5 Gbit/s signal at low error rate. It seems trivial today, but then it wasn't. Sometimes I wish my future self could have gone back and told my past self a few things that would have saved me years. We did some ideas all wrong, like tuning signals to have zero chromatic dispersion. Eventually, our Bell Labs colleagues helped us figure out that nonlinear interactions made zero dispersion a bad thing.

OSA: *When did wavelength-division multiplexing come in?*

NB: As soon as we got a single channel working, we started playing with WDM. Our first WDM test was only four channels, each at 2.5 Gbits for a total of 10 Gbits. When we realized that channels interacted, we added dispersion management. New transmission formats helped us increase higher data rates. We did some of the first experiments on forward error correction. Those were exciting and frustrating times with very long hours. I joke that I wandered into the lab one day and walked out seven or eight years later.

The introduction of a practical coherent transponder was the third basic paradigm shift. Originally, direct detection just turned a light on for one and off for zero, on-off keying up to billions of times a second. Coherent detection was tried in the early 1980s, but it didn't work because we couldn't lock the local oscillator to the signal frequency. Now, we get the two frequencies just close enough that fast sampling and digital signal processors (DSPs) can track the phase digitally and unscramble everything.

OSA: ***What's the capacity of today's transatlantic systems?***

NB: In round numbers, each fiber pair contains 100 WDM channels each carrying a 100 Gbit/s coherent signal, or 10 Tbit/s. A typical transatlantic cable can hold up to eight fiber pairs, so it can carry 80 Tbit/s. That is seven orders of magnitude larger than the capacity of the first submarine telephone cable that went into service 60 years ago. Many of our submarine systems are undersea networks running parallel to continental coastlines, with add/drop cables connecting to onshore locations (see figure). Because each fiber pair has huge capacity, it makes sense for users to share that capacity, as in terrestrial networks.

We use large-effective-area fibers with very low loss, the highest-performing type available. They have a lot of chromatic dispersion, but with coherent transponders the DSPs can do the dispersion compensation digitally. The high dispersion also keeps channels from interacting with each other, improving transmission quality.

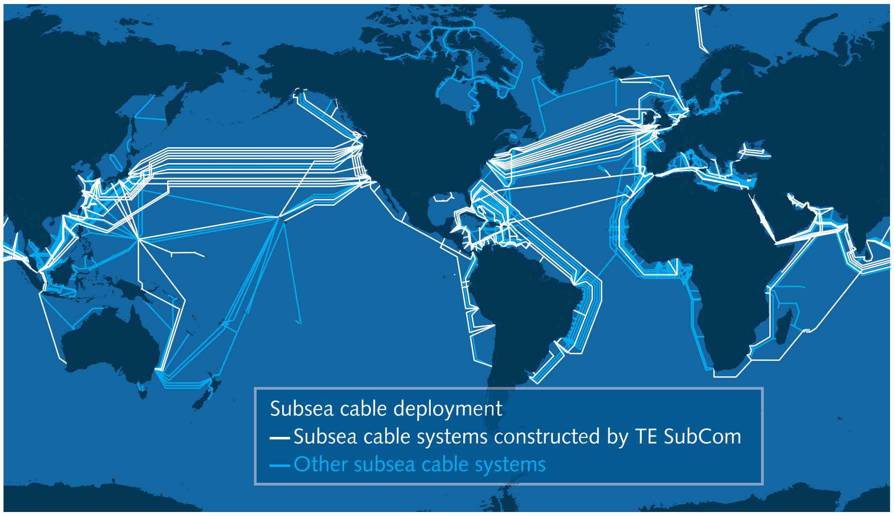

Many submarine systems are undersea networks running parallel to continental coastlines, with add/drop cables connecting to onshore locations. *(Adapted from TE Connectivity SubCom)*

OSA: ***What is the role of fiber in our increasingly mobile world?***

NB: We always think of cell phones as wireless communications devices. But 99% of the distance the signal travels between phones is on fiber-optic cable. Wireless transmission is only for a mile or two to the cellphone tower; then, fiber carries it the rest of the way. So the entire wireless system is built on fiber optics. The mobile network is a misnomer—users are mobile, but cell sites and cables are fixed.

OSA: ***Where do we go from here?***

NB: We are getting within factors of five or six of the fundamental Shannon limit on capacity of a single fiber mode. But good engineering will grow capacity because that limit is spectral efficiency-defined in bits per second per hertz of optical bandwidth. So we can increase capacity by using more optical bandwidth.

Other techniques can increase cable capacity by orders of magnitude. Capacity will scale with the number of modes you can get into a core, the number of cores in a fiber, and the number of fibers in a cable. That's because the Shannon limit is for a single mode, not a fiber or cable. So I remain a complete optimist. We won't be breaking any fundamental laws of nature, but we don't need to.

When I talk about the future, I think of when we celebrated the 35th service anniversary of a colleague last year. We started together and now that I'm the CTO, they invited me for cake and coffee. When it came time for me to say something, I recalled that another guy in the room had started that week. So I turned to the new guy and said, "I wonder what a communication system will look like when you celebrate your 35th anniversary in the year 2050." Imagine a multimode fiber with a coherent image processor, and every pixel in the image plane being a receiver. It sounds impossible today, but that will change when someone figures out how to do it.

The Optical Society celebrates a century of innovation

Throughout a century of breakthroughs, The Optical Society has brought together the best minds in optics and photonics to light the future. This series reflects on that history and looks to what innovations lie ahead. For more information, please visit http://osa.org/100.

Design approach to integrated photonics explores entire space of fabricable devices

ALEXANDER Y. PIGGOTT, JESSE LU, and JELENA VUČKOVIĆ

Knowing only the desired functionality, 'objective first' software designs smaller, optimized silicon photonic devices.

The design of digital circuits is currently dominated by hardware-description languages such as Verilog and VHSIC Hardware Description Language (VHDL). This automation of circuit design has enabled the development of modern computer processors with billions of transistors.

Integrated photonic devices, on the other hand, are still designed by hand. A designer first picks a basic design based on analytic theory with a handful (two to six) of free parameters. A canonical example would be the microring resonator (see Fig. 1), commonly used as a narrow spectral filter. The design is simple, with only a few adjustable parameters: the radius (*r*) of the ring, the width (*w*) of the waveguides, and the gap (*g*) between the ring and the waveguide. The designer then tunes these parameters by running many optical simulations. This brute-force approach is inefficient and limits the designer to a small library of known devices.

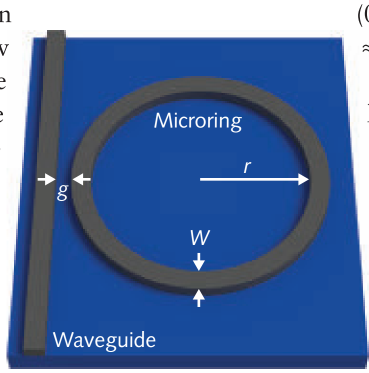

FIGURE 1. Shown is a schematic of a microring resonator, commonly used in integrated photonics. This resonator consists of a waveguide formed into a closed ring, which acts as a resonant cavity, and an input/output waveguide. The main design parameters are the ring radius (*r*), the waveguide widths (*w*), and the gap (*g*) between the input/output waveguide and ring.

Arbitrary photonic devices

What if, however, we were able to search the full space of fabricable devices? If we could do this successfully, we would be guaranteed to improve device performance and shrink device sizes. Unfortunately, the space of fabricable devices is absolutely enormous. For example, suppose we want to design a silicon photonics device with a 1 × 1 μm design region. If we divide it into 0.1 × 0.1 μm pixels, easily achievable with modern nanofabrication, and allow each pixel to either contain silicon (1) or not (0), then we have $2^{100} \approx 10^{30}$ possible devices.

We can draw two key insights about full-freedom design from this example. First, full-freedom design must be automated. A human designer would specify the device performance, but the actual design must be performed by a computer algorithm. Secondly, a simple brute-force search of all possible devices is intractable. Far more efficient design methods are necessary.

Ideally, we'd want an optimization algorithm whose computational cost is independent of the number of free parameters in the design. This would allow us to design devices that exploit the full space of fabricable devices. Thankfully, it turns out that such optimization methods exist. Related methods have long been used in other fields such as aerospace design and machine learning, but they were only recently introduced to optical design.

Design algorithms

Our research group uses two such methods to design arbitrary photonic devices. We first generate an initial guess for our structures using a so-called objective first design method.[1] In this method, we initially allow our electromagnetic fields to be unphysical, but force them to satisfy any performance constraints we may have. We then iteratively reduce any violation of Maxwell's equations by modifying both the structure and electromagnetic fields. Since we prioritize our performance objectives over Maxwell's equations, we call this method "objective first."

Next, we fine-tune our structures using the adjoint optimization method, which has also been studied by a number of other groups in the context of optical devices.[2-4] The key idea is that the gradient of a performance metric can be efficiently computed by simulating a single adjoint problem. This gradient can then be used in steepest-descent optimization. Adjoint optimization is essentially the opposite of the objective first method: here, we force Maxwell's equations to hold, and then try to minimize the violation of our performance constraints.

The vast majority of the computational cost for both methods comes from running a handful of electromagnetic simulations (as few as two) on each iteration. Critically, the number of simulations run on each iteration is completely independent of the number of free design parameters. This makes the objective first method and adjoint optimization far more efficient than heuristic methods such as genetic algorithms and particle swarm optimization, whose computational cost is proportional to the number of free parameters.

Both the objective first and adjoint optimization methods are iterative methods that converge on some local optimum. As such, neither method can find the globally optimal device for any given problem. However, by massively opening up the parameter space, we found that we can design devices with higher performance or a much smaller size than those designed using traditional methods.

One such device we designed using our algorithm is a TE/TM polarization splitter (see Fig. 2).[1] This device splits the two incident polarizations of light into separate output waveguides within a footprint of 2.8 × 2.8 μm. In simulations, it has an insertion loss of only 0.9 dB and a crosstalk of less than 19 dB.

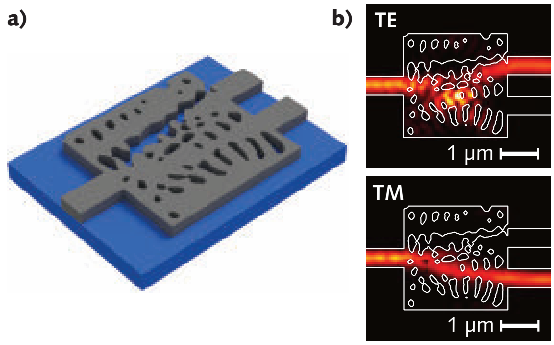

FIGURE 2. A polarization splitter for 1550 nm light is made from silicon and embedded in silicon dioxide (a). Simulated electromagnetic fields are shown for incident light that is horizontally (TE) and vertically (TM) polarized (b).

Experimental demonstration

As a proof of concept, we designed and experimentally tested a compact demultiplexer for telecommunications wavelengths (see Fig. 3).[5] This silicon photonics device splits 1300 nm and 1550 nm light with a device footprint of only 2.8 × 2.8 μm. The demultiplexer has an insertion loss of 2 to 4 dB, crosstalk less than 11 dB, and a 3 dB

bandwidth greater than 100 nm.

We also found that our demultiplexer was robust to fabrication imperfections. Despite being fabricated with minimal process control, our fabricated devices had highly repeatable performance (see Fig. 2). We achieved this by designing the device to be broadband, which we found was a good heuristic for fabrication robustness.[1]

Advanced optimization methods, combined with recent improvements in computational power, have started to change how we design integrated photonics devices. Using these methods, researchers have recently designed devices that can radiatively cool themselves below ambient air temperature even when exposed to direct sunlight,[6] or can make incandescent light bulbs nearly as efficient as LEDs.[7] In the future, we can expect sophisticated optimization methods such as our objective first method to revolutionize the photonics industry, enabling a new generation of extremely compact and high-performance optics. ◀

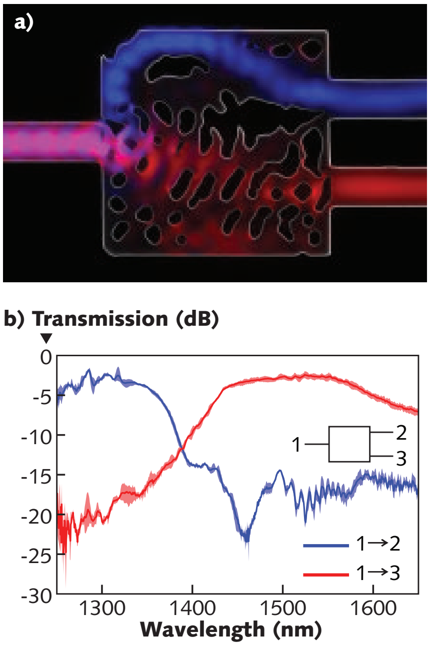

FIGURE 3. An electron micrograph of the compact demultiplexer device is overlaid with simulated electromagnetic fields at 1300 nm (blue) and 1550 nm (red), showing its effectiveness (a). The transmission was experimentally measured (b) from the input port 1 to output ports 2 (blue) and 3 (red). The average transmission is indicated by the solid lines, and the minimum and maximum values are indicated by the shaded areas. *(Adapted from A. Y. Piggott et al. with permission[5])*

REFERENCES

1. J. Lu and J. Vučković, *Opt. Express*, 21, 11, 13351–13367 (2013); doi:10.1364/oe.21.013351.
2. C. M. Lalau-Keraly et al., *Opt. Express*, 21, 18, 21693–21701 (2013); doi:10.1364/oe.21.021693.
3. A. C. R. Niederberger et al., *Opt. Express*, 22, 11, 12971–12981 (2014); doi:10.1364/oe.22.012971.
4. J. S. Jensen and O. Sigmund, *Laser Photon. Rev.*, 5, 308–321 (2011); doi:10.1002/lpor.201000014.
5. A. Y. Piggott et al., *Nature Photon.*, 9, 6, 374–377 (2015); doi:10.1038/nphoton.2015.69.
6. A. P. Raman et al., *Nature*, 515, 540–544 (2014); doi:10.1038/nature13883.
7. O. Ilic et al., *Nature Nanotechnol.*, published online Jan. 11, 2016; http://dx.doi.org/10.1038/nnano.2015.309.

Alexander Y. Piggott, **Jesse Lu**, and **Jelena Vučković** are at the Ginzton Laboratory of Stanford University, Stanford, CA; e-mail: piggott@stanford.edu; https://ginzton.stanford.edu.

Kilowatt-level fiber lasers mature

JOHN WALLACE, Senior Editor

Although today's high-power CW fiber lasers have their origins in telecom technology, they have long since left that arena and become naturals at reliable, capable materials processing.

Fiber lasers combine active (laser-gain) optical fiber with one or more pump lasers, usually laser diodes. The many types of fiber lasers include low-power continuous-wave (CW) and low- and high-energy pulsed, including ultrafast fiber lasers. But what comes to mind for many people are the "big guns"—the kilowatt-class CW fiber lasers that are predominantly used in materials processing, including cutting, welding, brazing, surface treatment, and other applications, but are also being developed for the military as directed-energy weapons.

A fiber is essentially a very skinny, long rod—its configuration makes it one of two types of lasers that have an especially high surface area-to-volume ratio, making them easier to keep cool (the other is the disk laser—a wide, extremely short rod). Fiber lasers are relatively simple in their construction and are easy to maintain. They are compact and, because they are pumped with laser diodes, rugged and long-lived.

Large range of powers and wavelengths

Alexei Markevitch, market development manager at IPG Photonics (Oxford, MA), outlines the range of wavelengths and powers available for kilowatt-class fiber lasers. "IPG manufactures standard kilowatt-class CW lasers at 1 μm (ytterbium-doped fiber) and 1.5 μm (erbium-doped fiber) and also manufactures custom kilowatt-class lasers at 2 μm (thulium doped fiber), along with lasers that have Raman-shifted wavelengths between 1.1 and 1.7 μm," he says. "The longer wavelengths enable nonmetal materials processing and other new applications and are considered to be eye-safe, as the eye-damage threshold is many orders of magnitude higher than for 1 μm lasers."

Markevitch notes that the kilowatt-class fiber laser systems operate in CW or modulated modes up to 5 kHz, and have dynamic range from 10% to full power with no change in beam divergence or beam profile.

At 1 μm, the company's single-mode YLS-SM ytterbium-doped fiber lasers span a power range from 1 to 10 kW, says Markevitch. These single-mode systems are used in advanced materials-processing applications requiring extremely high power and brightness, such as fine cutting and surface structuring, cutting high-reflectivity metals, microwelding, sintering, and

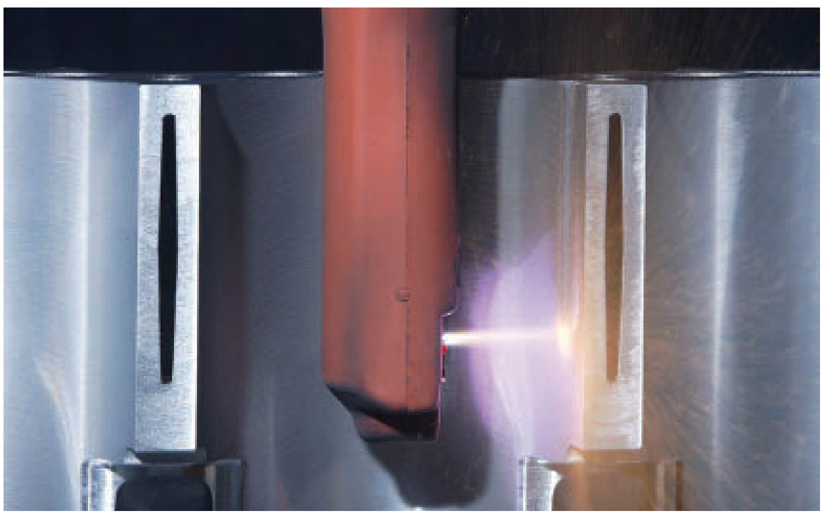

FIGURE 1. The cylindrical surface of a bore for an automobile engine is micromachined using a 2 kW single-mode fiber laser from IPG Photonics, then sprayed with plasma to create a hard coating that replaces conventional cylinder liners. Laser-machined microgrooves help the resulting coating to adhere to the cylinder. *(Courtesy of IPG Photonics)*

engraving, as well as remote processing and directed-energy applications.

"[IPG's] multimode YLS ytterbium-doped CW fiber lasers span a power range from 1 to 100 kW and can be manufactured up to several hundreds of kilowatts upon customer request," says Markevitch. "Their many uses include cutting, drilling, brazing, welding, annealing, heat treating, and cladding. With continuous improvement in their design, wall-plug efficiencies of standard industrial YLS system have now reached over 40%, and the industry record YLS-ECO series has a WPE exceeding 50%."

The same multimode YLS lasers are used for both high and low-brightness applications such as welding, drilling, and precision cutting—"a previously unheard of capability," Markevitch says. "The high brightness allows the use of long-focal-length processing lenses for vastly improved depth of field and minimal damage to optical components."

While high-brightness multimode lasers dominate in materials-processing applications, single-mode kilowatt-class CW lasers are gaining increasing attention, as they enable new applications that require high CW peak power with very small spot sizes and/or remote processing capability. Some applications of YLS-SM lasers described by Markevitch include high-speed slitting of stainless metals for sieves and filters, remote cutting of anode and cathode battery foils, remote and gas-assisted high-speed cutting of copper (Cu) and aluminum (Al) foils, and high-aspect-ratio narrow welding for minimal distortion of thin metals.

One particular example of kilowatt-class CW single-mode laser use highlighted by Markevitch is microstructuring of cast-iron and aluminum engines in the automotive industry. Environmental regulations requiring lower energy consumption as well as reduced pollution and carbon dioxide emissions create demand for thinner, lightweight engines. A new design for motor blocks with reduced wall thickness, aided by laser materials processing, results in 1 kg weight savings per cylinder.

To achieve higher mechanical resistance and optimize heat conductivity, the cylinders are sprayed with thin plasma coatings (see Fig. 1). Prior to the application of the cladding, the cylinder surface is microstructured with grooves that have a typical feature size of 100 μm or less.

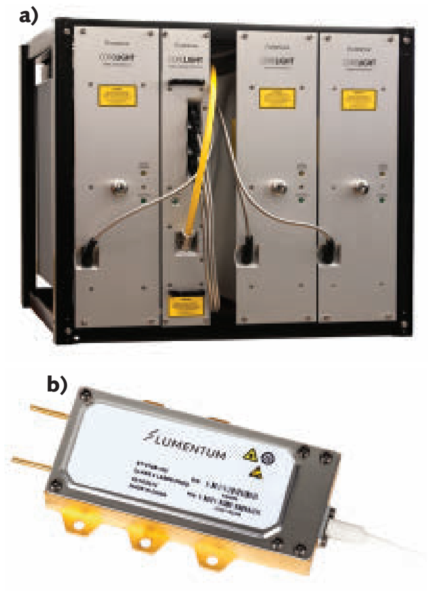

FIGURE 2. A 6 kW Lumentum fiber laser consists of three 2 kW modules and a fiber-combiner module (a). The lasers are pumped with the company's ST Series high-brightness fiber-coupled laser diodes (b). *(Courtesy of Lumentum)*

Such surface structuring has traditionally been done by mechanical or water-jet processing. These legacy technologies have various drawbacks. For example, mechanical processing is slow, can be done only perpendicular to the surface, and requires a change of tools for processing different parts and groove sizes. A water jet has very high power consumption (120 kW per nozzle) and high water consumption (contaminating water with Al), creates a sponge effect in Al, requires drying in a vacuum chamber, and can only be done on Al parts.

"A single-mode YLS-2000-SM laser with nominal power of 2 kW can treat both iron (Fe) and Al parts, is easily adaptable to treatment of parts of different diameter with grooves of different sizes down to 30 μm, and has a maximum power consumption of 5.5 kW," explains Markevitch. "Different groove angles are also possible. Both quality and throughput are much improved over traditional technologies."

Modular design

Erik Zucker, senior director of laser products and technology at Lumentum (Bloomfield, CT) describes both the modular nature and the inner workings of the company's Corelight kilowatt-class CW fiber-laser line. "Our basic building block is a double-clad fiber, single-oscillator module with over 2 kW output power," he says. "Several of these modules may be combined to provide significantly higher power from a single beam. Our fiber lasers are predominantly used for 2D sheet-metal cutting of materials ranging from mild and stainless steels to aluminum, copper, and brass. They can also be used for metal welding, brazing, and cladding applications."

The 2 kW fiber-laser module is made up of a single fiber oscillator that is end-pumped by an array of Lumentum's ST Series high-brightness, fiber-coupled laser diodes, which are designed and manufactured in-house, notes Zucker (see Fig. 2).

"Each pump produces 140 W of output power from a 106-μm-diameter fiber at over 50% wall-plug efficiency," he explains. "Multiple pump fibers are fusion-combined together into a single fiber, which in turn is spliced to one end of the oscillator. Fiber Bragg gratings define the cavity and output coupler. Because the 2 kW is produced from a single module, the beam-parameter product (BPP) is very low, typically 0.8 mm-mrad. This allows a small spot diameter with large depth of field to be focused on the workpiece in metal-cutting applications, which in turn creates a very high intensity and leads to extremely efficient cutting."

Zucker notes that 25-mm-thick mild steel can be cut with the 2 kW output from Lumentum's fiber laser, whereas a 4 kW CO_2 laser can only cut steel up to a 22 mm thickness. The low BPP leads to fast cutting: for example, 1-mm-thick aluminum can be cut at 75 m/min with 4 kW, while the 6 kW version cuts 1-mm-thick stainless steel at 94 m/min.

Amada (Kanagawa, Japan), a development partner and customer of Lumentum, incorporates the 2 kW laser into its cutting tools. One feature enabled in part by the low BPP of the 2 kW laser is called ENSIS, which allows on-the-fly electrical adjustment of the beam spot size on the workpiece. For automated cutting jobs, says Zucker, ENSIS can adjust from thin to thick metal cutting without operator intervention, improving productivity at job shops.

Getting the light to the workpiece

Rofin-Sinar Laser GmbH (Hamburg, Germany), which makes CW high-power fiber lasers (FL Series) ranging from 500 to 8000 W in output power, provides a number of ways to get light from the laser to the workpiece. The company's lasers can be supplied with either direct-spliced fiber of single-mode or multimode beam quality, or with a fiber-to-fiber coupler or fiber-to-fiber switches of multimode beam qualities, which allow the user to plug up to four fibers for sequential or parallel beam use, says Wolfram Rath, product manager laser sources at Rofin.

The spliced version is more compact, with a single cabinet, while the switched version has a separate enclosure for beam management. The lasers are used for cutting, welding, and surface treatment, as well as for a variety of scanner-based applications that are supported by integrated scanner processing.

The FL Series fiber lasers use a large-mode-area double-clad fiber as their active medium, says Rath. "These consist of an active single-mode core and a cladding with large diameter, in which the pump beam is conducted," he notes. "The pump light from long-life pumping modules is fed to the cladding from both sides by means of pump couplers. They are passively cooled, tolerating individual single faults, and can be exchanged in the field if necessary. The resonator mirrors are formed by inscribed fiber Bragg gratings (FBGs)."

The laser reaches an output power of 2.4 kW from a single fiber laser module, with a nominal power of 2 kW. Up to four fiber laser units can be combined by an all-fiber power combiner for a total nominal power of 8 kW, which can be delivered by up to four 100-µm-core-diameter process fibers to the processing cell.

These high-power fiber lasers are a standard tool for metal laser cutting and welding within the macro application branch, says Rath (see Fig. 3). Standard cutting systems are typically equipped with compact fiber lasers having direct process fiber of 50 µm or 100 µm core size depending on the power and sheet-thickness range of the cutting systems. "Welding of automotive parts is realized frequently within several workstations that are connected to the laser by different fiber cables that can be as

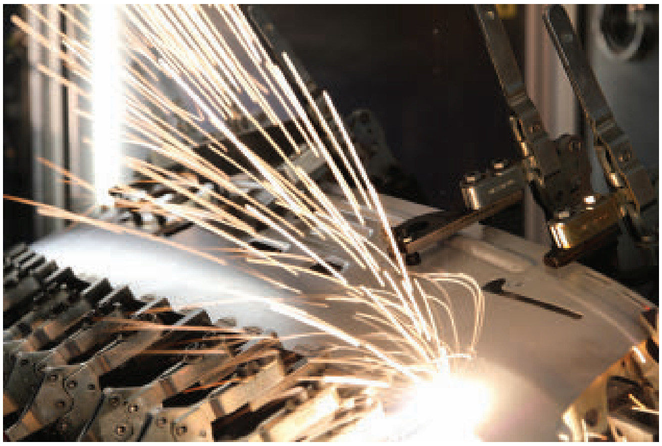

FIGURE 3. A Rofin scanner-based fiber laser welds automotive parts. *(Courtesy of Rofin-Sinar)*

long as 100 m," Rath says. "This setup helps to minimize the cycle times and optimize the laser utilization. For example, the parts are assembled and clamped in station 'A' when the laser is welding a second workpiece at station 'B.'"

Because the fiber laser can be adapted to the application by choosing the fiber size, the same laser can be used for different operations. For example, manufacturing of an automotive part is done using three different laser-processing methods that are performed subsequently in three working cells: coating removal (performed using a high beam quality and integrated scanner processing), cutting of an aperture for perfect fit, and welding.

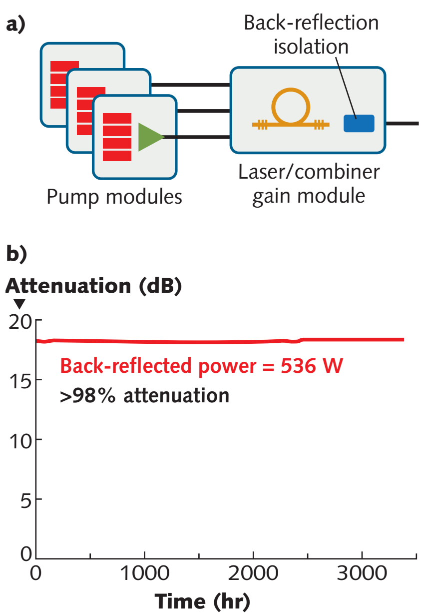

FIGURE 4. The nLIGHT alta design incorporates a back-reflection isolator between the laser and delivery fiber (a). A continuous laser-stability stress test with greater than 500 W directed back into the laser for thousands of hours shows no indication of unstable operation (b). *(Courtesy of nLIGHT)*

Back-reflection isolation

Kilowatt-level industrial fiber lasers that perform operations on highly reflective materials are faced with the problem of back reflection, where light reflected from the laser optics' focal region on the workpiece passes backward through the laser system. "Typical back reflections are only a fraction of the laser power because of work-piece surface irregularities, lack of precise alignment with the

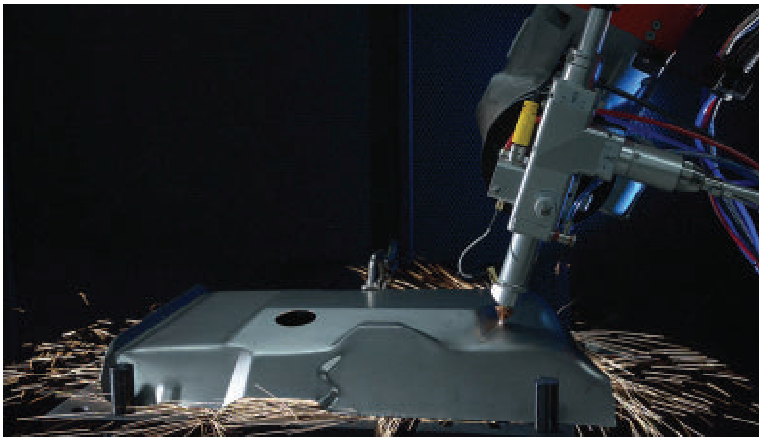

FIGURE 5. A Coherent Highlight FL fiber laser can be combined with robotics to enable high-speed 3D part cutting for industries such as white goods (washing machines, kitchen stoves, and so on). *(Courtesy of Coherent)*

surface normal, and the limited collection angle of the process optics; furthermore, in many cases the back reflection has a short duration (for example, piercing)," says Jake Bell, general manager at nLIGHT (Vancouver, WA). "Nonetheless, the design of some fiber lasers renders processing of reflective materials difficult or impossible."

nLIGHT produces a series of materials-processing fiber lasers with power levels ranging from 500 W to 4 kW. Among other attributes, the nLIGHT alta series has a unique configuration to minimize back reflection. "Damage caused by back reflections usually results from deposition of optical power into polymer materials, which overheat and burn," explains Bell. "The nLIGHT alta strips the back-reflected light coupled into the feeding fiber and directs it to a water-cooled beam dump where it is converted to heat without any interaction with polymers, thereby eliminating the primary damage mechanism. The polymer-free isolator is designed to dump more than 500 W continuously (see Fig. 4)."

Bell says, "We evaluated the performance of the isolation system in the case of piercing, where the highest back-reflection signals occur in laser cutting. The test successfully processed 4000 consecutive pierces of copper with no interruptions or failed pierces. In contrast to the robust, hardware-based protection provided by our back-reflection isolator, some other fiber lasers employ software protection that disables the laser in the case of a back reflection; this approach may protect the laser, but it precludes successful continuous materials processing."

The back-reflected light that is dumped in the isolator is monitored using a photodiode, says Bell. The real-time output of this sensor is provided to the user for use in process monitoring, optimization, and control (for example, pierce detection) or for tool calibration (such as beam position and focus).

Other qualities of the nLIGHT alta lasers outlined by Bell include improved cutting and welding performance, in which the

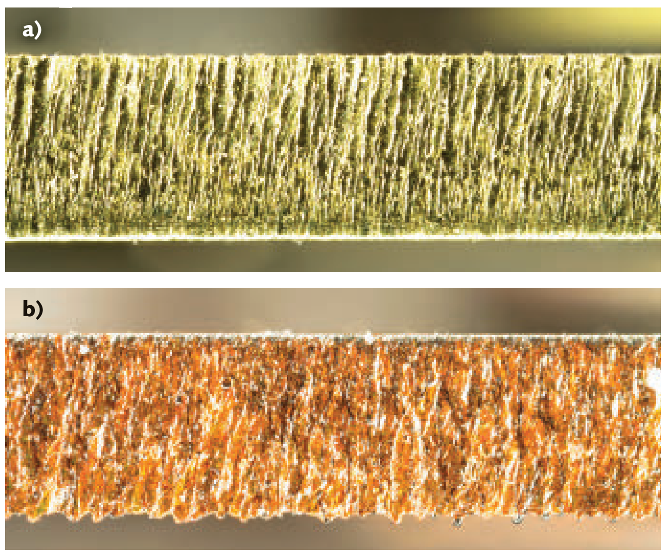

FIGURE 6. Immunity from back-reflections enable cutting of highly reflective metals that were problematic for first some-generation fiber lasers. Cross-section views show cuts created by a Coherent Highlight FL laser through 1.25-mm-thick brass (a) and 1.2 mm copper (b). *(Courtesy of Coherent)*

lasers can deliver a modulation rate up to 100 kHz and a rise and fall time of less than 5 μs. These capabilities allow faster piercing, faster processing of fine features, and better processing quality through minimal heat affected zone, he says.

"Most multi-kilowatt fiber laser systems employ an architecture based on combining the outputs of multiple, lower-power fiber lasers, resulting in significant shortcomings in cost, performance, serviceability, upgradeability, and amenability to technological advances," he adds. "We introduce a novel kilowatt fiber-laser architecture that solves these problems by housing the pump diodes and drivers in standalone pump modules and the gain fibers in a configurable gain module that can generate more than 4 kW of output power."

These lasers, which have tailorable beam quality (BPP ≥ 1.1 mm-mrad), have been used for high-quality cutting and welding of mild steel, boron steel, stainless steel, aluminum, brass, and copper, and have also been employed in emerging applications that include additive manufacturing and surface texturing and engraving.

Quick component replacement or upgrade

As described by Frank Gaebler, marketing director for materials processing at Coherent (Santa Clara, CA), first-generation fiber lasers were based directly on telecom platforms massively scaled to higher power, using a large number of separate pump laser diodes, each independently fiber coupled and permanently spliced together.

"This brute-force approach to higher power has several limitations," he says. "In particular, all the components are permanently spliced together. If one component fails or degrades, there is no way to replace it. For example, early models were found to be susceptible to back reflections from metal processing. If the fiber splices, pump diodes, delivery fiber, or any other laser component is damaged by such back reflections, the laser had to be factory-repaired or exchanged, negatively impacting uptime and net production.

Coherent makes a second-generation kilowatt-scale fiber platform (the Highlight FL) based on a flexible modular architecture (see Fig. 5). Engineers at Coherent have used a substantially different design approach that eliminates the complexity of multiple pumps and splices, with a modular architecture that also enables simple replacement and/or upgrade of the various components, including the delivery fiber, notes Gaebler.

We use fiber-coupled high-power laser-diode bars rather than multiple separate laser diodes," he says. "Their output is then coupled into the gain fiber using free-space coupling; this coupling module is also used to connect the gain fiber to the detachable delivery fiber." He adds that this approach is particularly attractive to OEM system builders, as they can buy complete lasers or separate modules depending on their level of expertise or requirements for deep integration, and they can quickly change or replace the delivery fiber to suit different applications.

In terms of specifications, at present, Coherent's Highlight FL fiber lasers are targeting steady increases in maximum power, says Gaebler: the latest model delivers 3 kW with an increase to 4 kW expected sometime in 2016. "At present, our delivery fiber modules are available with a 100 μm core, which corresponds to a BPP of around 4 mm-mrad," he says. "A 50-μm-core delivery fiber has recently become available for some models that can achieve a reduction in BPP of up to 2X. As a result of their high power and low BPP, these HighLight FL lasers are well-suited for processing metals ranging in thickness from thin foil to a few millimeters."

Early fiber lasers sometimes struggled to cut, drill, and weld certain metals, notes Gaebler. For example, fiber-laser fundamental output wavelengths are usually around 1 μm. This is a wavelength region where brass and copper exhibit very high reflectivity, as evidenced by the extensive use of copper mirrors for beam delivery of near-infrared lasers of all kinds. Retroreflections have made these metals a significant challenge for machining with first-generation fiber lasers.

According to Gaebler, unlike first-generation fiber lasers, the Highlight FL laser architecture is immune to back-reflection damage for two reasons: 1) the geometry and optical properties of the dichroic beam combiner mean that any back reflections cannot reach the pump diode bar; and 2) there are no fiber splices to be damaged by any back reflections. As a result, the lasers are not limited by qualifiers that urge extreme caution with reflective metals (see Fig. 6).

For More Information

Companies mentioned in this article include:

Coherent
Santa Clara, CA
www.coherent.com

IPG Photonics
Oxford, MA
www.ipgphotonics.com

Lumentum
Bloomfield, CT
www.lumentum.com

nLIGHT
Vancouver, WA
www.nlight.net

Rofin-Sinar
Hamburg, Germany
www.rofin.com

FOR A COMPLETE LISTING OF COMPANIES *making high-power fiber lasers, visit the* Laser Focus World *Buyers Guide (http://buyersguide.laserfocusworld.com/index.html).*

Femtosecond laser optics combat pulse dispersion, color errors, and reflections

GÜNTER TOESKO and CHRISTIAN DEHNERT

Along with the rapid development pace of ultrafast lasers, ultrafast laser optics must overcome the unusually amplified obstacles of dispersion, color aberrations, and ghost reflections through careful design and manufacture.

The pace of the development of ultrafast lasers—also called ultrashort pulse (USP) lasers—has been extremely rapid. Picosecond and femtosecond laser systems are efficient tools in many industrial and scientific applications, offering useful nonlinear effects and "cold ablation" for a reduced heat-affected zone (HAZ) that reduces or even eliminates post-processing cleanup in materials processing applications.

Besides multiphoton absorption and self-focusing in transparent materials for improved outcomes in ophthalmic (Lasik surgery) and biological applications, the nonlinear attributes of ultrafast lasers are also used to modify the index of refraction and distribute the laser energy along the beam axis to maintain a near-constant beam radius over many Rayleigh lengths, enabling a very large depth of field.

As a result, USP lasers are well suited to contour cutting (filament cutting) of uncured, chemically hardened glass (cover glass of smartphones) and sapphire, resulting in very high-quality edges and very little material removal. This plasma dissociation process leads to cutting kerfs smaller than 1 μm—much smaller than the diffraction-limited laser spot diameter.

So, what are the optical challenges with ultrafast lasers? Avoiding dispersion, color shifts, and ghost reflections in ultrafast laser optics are of primary importance in maintaining optimum system performance.

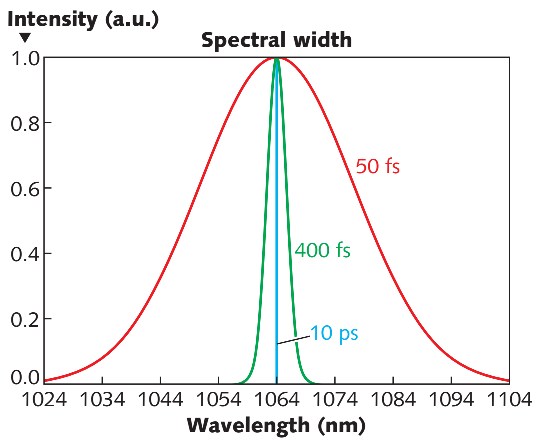

FIGURE 1. For ultrafast lasers, a formula defines the spectral width of a transform-limited pulse to be a function of the pulse duration. *(Courtesy of Sill Optics)*

Dispersion

Material dispersion in ultrafast laser optics leads to temporal broadening of the laser pulse by introducing a frequency-dependent delay of the different spectral components of the pulse. The higher the refractive index of a material, the higher the dispersion. In addition, the dispersion effect is greater for shorter wavelengths. For example, a 400-fs-long pulse with a central wavelength of 355 nm suffers a temporal broadening of approximately 0.3 fs while traveling through a 20-mm-thick fused-silica window.

In long-pulsewidth laser beams, the wavelength bandwidth is very narrow and typically no compensation is required in the lens. But as the pulse width shortens, the wavelength spread around the center wavelength increases—it is a function of the laser, not the lens.

Color aberrations

In femtosecond lasers, the pulse length is linked to the spectral width of a laser pulse. As the pulse width of a laser decreases into the range of femtoseconds, the pulse spreads out in frequency. For example, a 10 ps pulse at 1064 nm has a spectral width of about 0.3 nm, resulting in essentially no pulse spreading. At the other extreme, a 50 fs pulse at 1064 nm has a spectral width of about 60 nm, yielding much broader

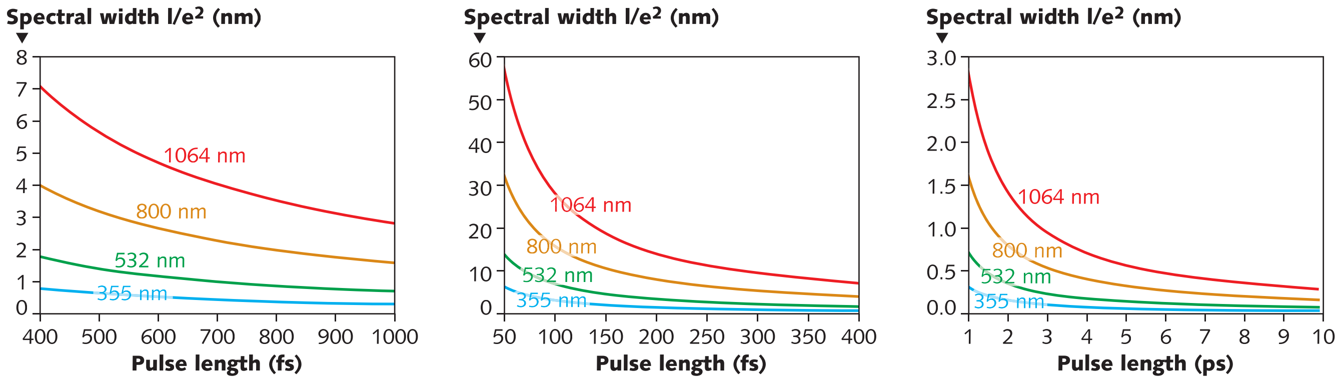

FIGURE 2. Spectral width increases with decreasing pulse length for a variety of pulse-length ranges; below 400 fs, the spectral broadening increases rapidly. Note the steeper slope of the longer wavelengths. *(Courtesy of Sill Optics)*

spectral content such that the pulse contains wavelengths from 1034 to 1094 nm, resulting in a "color error" unless the lens is color-corrected.

In USP lasers, the spectral width is defined by the pulse duration as:

$$\text{Spectral width [FWHM]} \geq \text{constant} * \frac{(\text{central wavelength})^2}{\text{pulse duration} * \text{speed of light}}$$

The constant (time-bandwidth product) depends on the actual pulse shape (see Fig. 1). For a Gaussian pulse shape, it is equal to 0.441. If equality is obtained in the above equation, then it is a transform-limited pulse, meaning that for a given spectral width, there is a lower limit for the pulse duration.

A problem most severe at longer wavelengths is that the shorter the pulse duration, the larger the spectral width of the pulse (see Fig. 2). For pulse lengths in the picosecond regime, the spectral width is around 1 nm and below, and can usually be neglected. In that case, fused silica lenses that are color-corrected monochromatically for just one wavelength can be used and only one glass material is required.

Color errors occur from the broad spectrum of the short-pulse input beam. Wavelengths are focused to different locations along the propagation direction (axial chromatic focal shift) and lateral to it (lateral chromatic color aberration) (see Fig. 3). The amount of the lateral color error is dependent on the focal length and the wavelength, as the image height ("scan length" when referencing F-Theta scan lenses) is proportional to the field angle (field height = focal length × field angle) and the field height is different for different wavelengths.

Correcting color errors

Most optical imaging lenses that span the human visible spectrum such as binoculars or machine-vision imaging lenses correct for color errors by combining various glass types with different indices of refraction and different Abbe numbers. The Abbe number is a measure of the material's chromatic dispersion—its variation of the refractive index vs. wavelength.

Nanosecond and picosecond pulse lasers have a very small spectral spread on the order of a few nanometers or less, resulting in essentially no wavelengths that are out of focus, both axially in z and laterally in the x and y scan field. In that case, fused-silica lenses designed for a single wavelength and corrected monochromatically can be used. However, femtosecond USP lasers are more challenging.

To illustrate the spectral bandwidth impact on the performance of an F-Theta scan lens, the Sill telecentric F-Theta scan lens S4LFT4010/328 with 100 mm focal length used with a 10 mm ($1/e^2$, vignetted at $1/e^2$) input beam and a maximum field size of 35 × 35 mm was analyzed (see Fig. 4). Unlike a normal focusing lens that has field curvature so only the center ray would be in focus on a flat field, an F-Theta scan lens is designed to be in focus over the entire image plane of the field scanned by the laser.

Designed for one wavelength only at 1064 nm, this F-Theta lens shows that spot performance in the corner of the scan field (a location at which the color errors are at their maximum) results in color errors both in the transverse (scan-length direction) and propagation direction (focal-length direction). At 400 fs, the spot shape is essentially the same as for a 10 ps or longer pulse, and the lateral color error is small in respect to the spot size. The image size of the Huygens point-spread function (PSF) plot is 40 µm and the lateral color error is approximately 8 µm. But at 50 fs, the lateral color error is approximately 60 µm and the aberrations are quite obvious and extreme.

To combat this color error, Sill Optics designed the proprietary, multi-element, multi-material S4LFT7010/450 telecentric F-Theta scan lens with a focal length of 100 mm and a maximum field size of 35 × 35 mm with color correction from 1.0 to

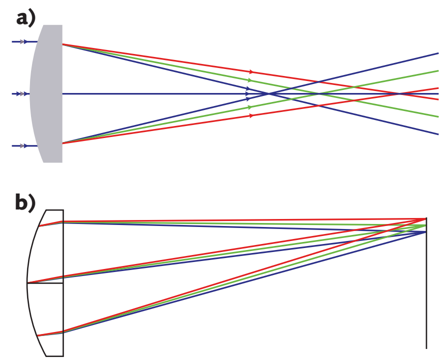

FIGURE 3. In lenses not corrected for color errors, chromatic focal shifts can occur axially (a) or laterally (b). *(Courtesy of Sill Optics)*

1.1 μm for a 100-nm-wide color spectrum. For a 10 mm beam, the lens is diffraction-limited (the maximum theoretical resolution possible) with a lateral color error in the field corner below 1 μm by design, resulting in a very round nonaberrated spot.

The S4LFT7010/450 is being used in the European-founded project ADALAM (grant agreement number 637045; http://www.adalam.eu) with a goal of developing an adaptive laser micromachining system based on USP laser ablation and a novel depth-measurement sensor, together with advanced data analysis software and automated system calibration routines.

Complementary with this new F-Theta scan lens, Sill Optics has also introduced the S6ASS4803/450 3X beam expander that is color-corrected from 1.0 to 1.1 μm and diffraction-limited for a 10 mm beam (double $1/e^2$ diameter).

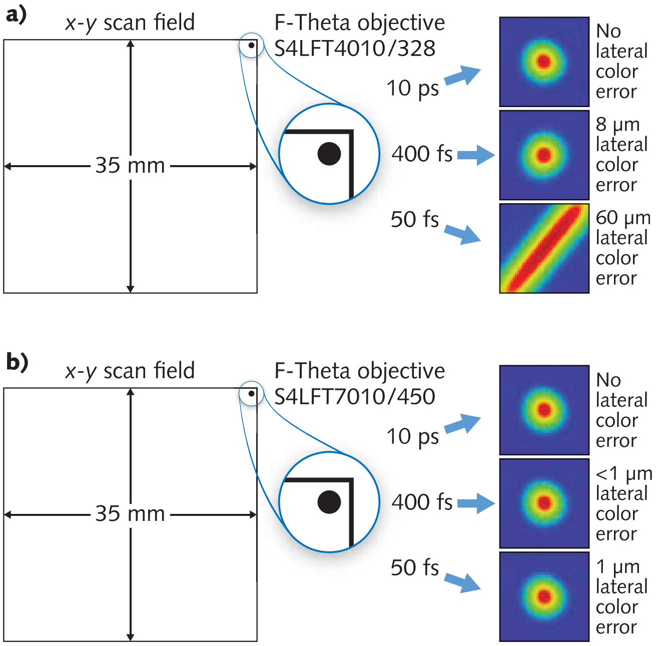

FIGURE 4. The Sill Optics S4LFT4010/328 monochromatic scan lens with a 35 × 35 mm scan field is used to demonstrate spot performance in the corner of the scan field for 10 ps, 400 fs, and 50 fs pulse widths. The spot is extremely distorted at 50 fs (a). But for the S4LFT7010/450 telecentric F-Theta lens with 100 mm focal length, the lens is diffraction-limited for a 10 mm beam and the lateral color error in the field corner is below 1 μm (b) by design, resulting in a very round nonaberrated spot. *(Courtesy of Sill Optics)*

Ghost reflections

Ghost (or back) reflections occur as a portion of the laser light is reflected back from various lens elements. Most F-Theta scan lenses contain anywhere from 2 to 6 lens elements. Because lens

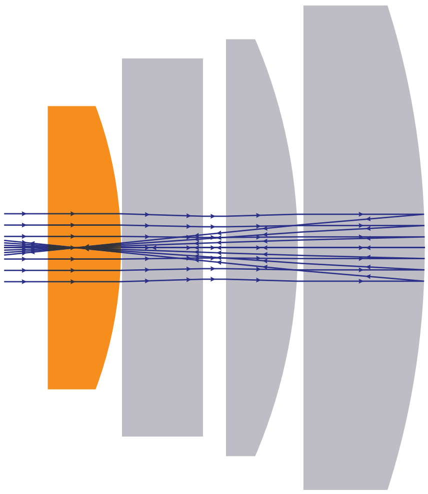

FIGURE 5. Back reflections on the outer surface of lens element four form a focus in the first lens element. In a pulsed laser, even a small amount of reflected energy can damage the coating. *(Courtesy of Sill Optics)*

surfaces typically reflect back about 4% of the light energy on each surface, laser lenses use antireflection coatings to transition the light from the index of refraction of the air to the refractive index of the bulk material of the lens (see Fig. 5), reducing the back reflection from each surface to about 0.2%. Although 0.2% seems like a small amount, the peak power of the ghost spot in a pulsed laser can exceed the damage threshold of the coating.

If the reflection is focused into the air space between lens elements or inside the bulk material of the lens, then it is not a problem. However, if the back reflection is focused onto the surface of a previous lens element or onto a galvo scan mirror surface, the energy density can burn a spot into the coating. The solution is an optical design that avoids these focused back reflections and maintains all the other constraints (focal length, scan field size, spot size, and glass types, among others) within the optical design. Back reflections onto the galvo scan mirrors are controlled by using the correct F-Theta lens adapter ring thickness.

Günter Toesko is senior project manager, laser components at Sill Optics, Wendelstein, Germany; e-mail: guenter.toesko@silloptics.de; and **Christian Dehnert** is applications and sales engineer at CourierTronics, Troy, NY; e-mail: cdehnert@couriertronics.com.

Pushing fiber line rates beyond 100 Gbit/s

JEFF HECHT, Contributing Editor

Superchannels now can transmit hundreds of gigabits/s long-haul distances on standard singlemode fiber. Large mode-area fibers can carry superchannels further and faster, and new multicore and few-mode fibers promise future advances.

Coherent transmission at 100 Gbit/s has become standard in the global fiber-optic backbone network, and more is coming. A few systems are operating at hundreds of gigabits, and hero experiments have exceeded a petabit (10^{15} bits/s) over single developmental fibers that can transmit light on dozens of separate paths. It may remind you of the explosive growth of the 1990s.

Yet today's picture is more complex because the technology is advancing on three fronts—existing systems based on step-index "standard" singlemode fiber, new systems using large mode-area fibers, and development of spatial-division multiplexing over new fiber types

Coherent transmission and digital signal processing are making the most of the 9-μm-core singlemode fiber used since the 1980s. Dark fibers installed during the bubble years remain widely available on North American and European routes. Today's long-haul coherent systems can transport 100 Gbit/s signals on close to a hundred 50 GHz optical channels on such fibers—a total of 10 Tbit/s per fiber pair—and new technology may offer some further increase.

Large mode-area fibers are preferred for new submarine and terrestrial cables. Their low nonlinearity allows them to carry higher data rates over longer distances.

In the longer term, developers are working on new fiber types that can multiply capacity by spatial-division multiplexing—using separate cores within a fiber and separate modes within few-mode cores. Potential applications include long-haul transmission and shorter distances, from within server farms to metro distribution networks.

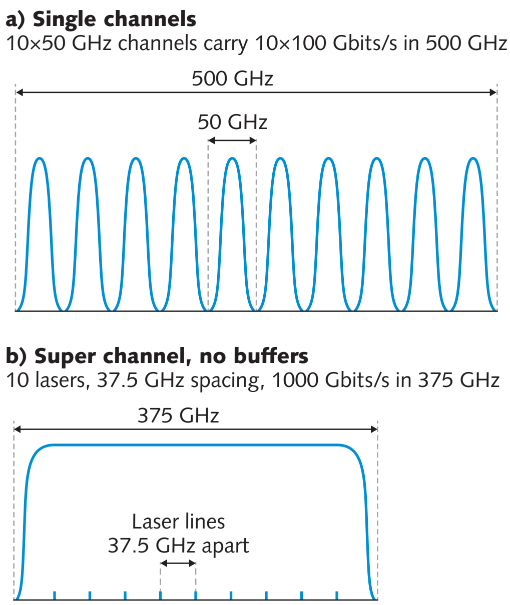

FIGURE 1. Transmission of 1 Tbit/s using ten 100 Gbit/s channels in 50 GHz slots (a) compared with a 1 Tbit/s superchannel using 10 lasers spaced at 37.5 GHz intervals across a 375 GHz range. The superchannel spans the band without buffer layers shown between the conventional 50 GHz channels (b).

Approaching the wall with standard singlemode fiber

Today's 10 Tbit/s capacity represents a factor-of-25,000 increase since standard singlemode fibers began carrying 400 Mbit/s in the mid-1980s. Ganging coherent transmitters together to form "superchannels" in multiples of 100 Gbit/s can increase capacity about another 30%. The trick is to combine signals from several laser transmitters, eliminating the buffer zones that separate traditional 50 GHz channels (see Fig. 1).

Demonstrated single-channel data rates have reached the terabit level. In 2014, Infinera (Sunnyvale, CA) sent a 1 Tbit/s superchannel signal 500 km through a loop of installed fiber between Budapest, Hungary and Bratislava, Slovak Republic. A single photonic integrated circuit contained the 10 laser sources. The prototype 1 Tbit/s line card can cover much longer spans using polarization-multiplexed quadrature phase-shift keying (PM-QPSK), says Geoff Bennett of Infinera. Using current production-level 500 Gbit/s line cards, Infinera and Facebook spanned 4000 km without regeneration. Bennett credited the improvement to splitting signal processing between transmitter and receiver in second-generation coherent systems.

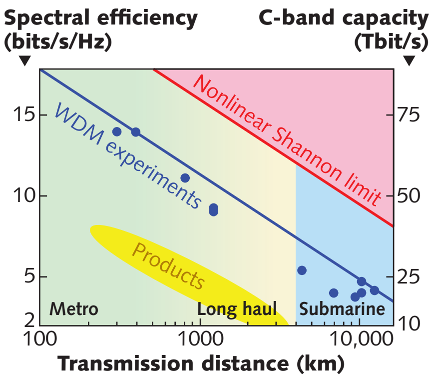

FIGURE 2. Standard singlemode fiber systems are closing in on the nonlinear Shannon limit, shown at upper right. The blue line shows experimental demonstrations and the yellow area commercial products. The vertical scales show capacity of the erbium-fiber C band (right) and spectral efficiency (left). *(Courtesy of Peter Winzer, Bell Labs[3])*

However, standard singlemode fiber is approaching the nonlinear version of the Shannon limit on error-free transmission capacity.[1] Noise imposes the traditional Shannon limit, so capacity of a linear medium can be increased by complex coding schemes that generate higher power to increase signal-to-noise ratio. However, optical fiber is a nonlinear medium, so the extra power from complex coding generates nonlinear noise. This decreases the signal-to-noise ratio and thus imposes a more stringent limit on transmission efficiency, usually measured as bits per second of signal per hertz of bandwidth. The result is an inherent tradeoff between coding rate and transmission range in a fiber (see Fig. 2).

Large-mode-area fibers carry more data

Large-mode-area fibers spread signals over a larger area, reducing power density and nonlinear noise. That extends transmission capacity and reach, so solid-core large-area fibers have become standard for new long-haul terrestrial and submarine cables. Both Corning (Corning, NY) and OFS (Norcross, GA) offer fibers with effective mode areas of at least 125 μm^2 and attenuation below 0.19 dB/km in the 1.55 μm band. Effective mode areas have reached over 1000 μm^2 in photonic-crystal fibers, but their loss is far too high for use in communications.

Large-mode-area singlemode fibers usually have a high chromatic dispersion. But that's no longer a problem because coherent transmission and digital signal processing have enabled powerful electronic dispersion compensation.

The spread of large-area fibers allows use of higher power and advanced coding techniques to increase data rates and distances. Ciena (Hanover, MD) sent a 1 Tbit/s superchannel with 16-QAM modulation carrying live traffic through nearly 1000 km of such fiber in the Comcast (Philadelphia, PA) long-haul network. Thanks to the advanced coding scheme, the spectral efficiency reached 5 bits/s/Hz. Bennett says that laboratory tests of low-mode-area fibers stretched the reach of PM-8QAM signals nearly a factor of three to transatlantic distances.

Large-area, low-loss fibers also have become standard for long-haul submarine cables, as Neal Bergano of TE Connectivity SubCom (Eatontown, NJ) mentions in this month's Future Optics interview (see page 21). Transoceanic cables with eight fiber pairs and advanced coding have capacity of 80 Tbits. In a recent experiment, Bergano's group transmitted 152 200 Gbit/s polarization-multiplexed 16-QAM channels with efficiency of 6 b/s/Hz through a 9748 km testbed.[2] But capacity is expected to top out about a factor of 10 above standard singlemode fiber.

At last year's Optical Fiber Communications (OFC 2015) conference, the postdeadline hero experiments session heard three reports of multimode transmission in each of several cores in multicore fibers.

Spatial-division multiplexing

For the long term, spatial-division multiplexing offers a potential hundred-fold capacity boost by sending signals on parallel physical routes between two points. Peter Winzer of Bell Labs calls it the fifth physical dimension of optical multiplexing, after time, phase, frequency, and polarization.[3]

Spatial multiplexing through separate fibers in the same cable is well established, but offers little prospect for integration of other components such as amplifiers. Multicore fibers and multiple-mode cores offer much more hope for integration, but they require extensive development. "We all know that parallel systems will happen. The question is which form of parallelism makes the most economic sense," says Winzer.

Early multimode and multicore tests were encouraging. At the 2012 European Conference on Optical Communications (ECOC), Nippon Telegraph and Telephone (Tokyo, Japan) sent a record 1010 Tbit/s (1.01 Pbit/s) through 52.4 km of a 12-core fiber.[4] Each core carried 380 Gbit/s on 222 separate wavelengths, a total of 84.5 Tbits per core. Modal-division multiplexing was demonstrated separately on few-mode fibers.

At last year's Optical Fiber Communications (OFC 2015) conference, the postdeadline hero experiments session heard three reports of multimode transmission in each of several cores in multicore fibers. Two described spatial division multiplexing through more than 100 paths on several kilometers of fiber. J. Sakaguchi of the National Institute of Information and Communications Technology (Tokyo, Japan) sent three modes through each of 36 cores in their 5.5 km fiber,[5] and Koji Igarashi of KDDI R&D Labs (Saitama, Japan) sent six modes through each of 19 cores of a 9.8-km fiber.[6] In a third paper, Kouki Shibahara and colleagues at NTT

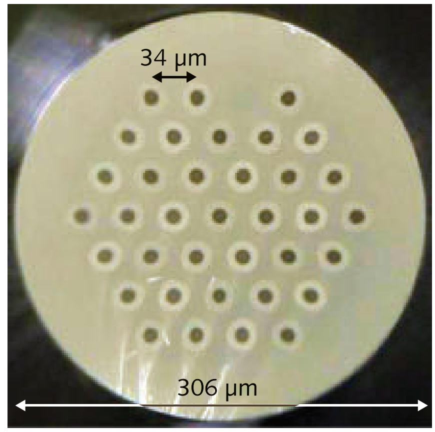

FIGURE 3. A 36-core fiber containing three different types of cores, each able to carry three modes, used in experiments at the National Institute of Information and Communications Technology in Tokyo. *(Courtesy of J. Sakaguchi et al.[5])*

Laboratories reported sending signals in three modes on each of 12 cores 10 times through a 52.7 km loop with an amplification stage. Demonstrating amplification, transfer of signals between fibers, and reaching a total distance of more than 500 km were important steps, although the NTT group used fewer levels of spatial multiplexing.[7]

Big questions remain. How much crosstalk will occur between modes in few-mode fibers during coupling and during amplification? How well can amplifiers and couplers be integrated? How much can spatial-division multiplexing increase efficiency measured in bits per second per hertz? How much spatial-division multiplexing will be possible over transoceanic distances?

Recent theoretical work hints at unexpected limitations. At the 2015 ECOC, Kasyapa Balemarthy and Robert Lingle of OFS warned that a 220 μm fiber could accommodate no more than 5–7 cores without degrading 100 Gbit/s signals after 6000–12,000 km.[8]


eagleyard
photonics
SENSE THE POWER
Brightness – beyond engineering.
www.eagleyard.com
20 Watt Peak Power @ 808nm
eagleyard's new 808nm broad area semiconductor laserdiode delivers 20 Watt peak power under pulsed operation from a single emitter.
· 10µs pulse width @ 25kHz Repetition Rate. T_{op} -40°C to +80°C
· Upon request also available with fast axis collimation (FAC)
Its high pulse energy and fast rise time makes this laser diode ideally suited for high resolution sensing applications in extreme harsh environments.
More Multimode laser diodes can be found under http://www.eagleyard.com/products/multimode-laser-diodes/

Outlook

The bottom line question is what technology offers the best value. The main attraction of integrating spatial division multiplexing is the potential to lower costs. Yet, as Winzer says, "Nobody can build a 19-core fiber at a lower cost than 19 individual fibers." So at best, multicore, multimode fiber is years from practicality.

Yet if you look back, in the late 1970s many people thought it would be more practical to lay many parallel multimode fibers than one singlemode fiber. In the 1980s, coherent transmission was deemed impractical, and would stay on the shelf for two decades before new technology opened the door to 100 Gbit/s coherent transmission. Other options also remain, including expanding the transmission spectrum beyond the 1530 to 1565 nm erbium-fiber C band. And stay tuned for any surprises at the OFC 2016 postdeadline sessions on March 24. ◀

REFERENCES

1. A. D. Ellis et al., "The nonlinear Shannon limit and the need for new fibres," *Proc. SPIE*, 8434, 84340H (Jun. 1, 2012); doi:10.1117/12.928093.
2. J.-X. Cai et al., *Opt. Express*, 22, 4, 9115 (Apr. 8, 2014); doi:10.1364/oe.22.009116.
3. P. Winzer, *Bell Labs Techn. J.*, 19, 22 (2014); doi:10.15325/bltj.2014.2347431.
4. H. Takara et al., "1.01-Pb/s (12 SDM/222 WDM/456 Gb/s) crosstalk-managed transmission with 91.4-b/s/Hz aggregate spectral efficiency," *Proc. ECOC*, Th.3.C.1 (Sept. 2012).
5. J. Sakaguchi et al., "Realizing a 36-core, 3-mode fiber with 108 spatial channels," *Proc. OFC*, Th5C.2 (2015).
6. K. Igarashi et al., "114 space-division-multiplexed transmission over 9.8-km weakly-coupled-6-mode uncoupled 19-core-fibers," *Proc. OFC*, Th5c.4 (2015).
7. K. Shibahara et al., "Dense SDM (12 core × 3 mode) transmission over 527 km with 33.2-ns mode-dispersion employing low-complexity parallel MIMO frequency domain equalization," *Proc. OFC*, Th5C.3 (2015).
8. K. Balemarthy and R. Lingle Jr., "Upper limits on number of cores for multi-core SMFs over trans-oceanic distances at 100Gbps," *Proc. ECOC*, 0761 (2015).

Scanning advances brighten and enhance laser light shows

JUSTIN PERRY

Once built primarily around bulky and expensive krypton lasers, the newest multicolor laser systems have taken advantage of improved scanning systems and advanced software programmability for enhanced laser light show experiences.

Optical scanners used to direct, position, or "scan" a laser beam over a desired area are in widespread use throughout the industrial, medical, and entertainment laser industries. Recent advances in galvanometer-based optical scanners can deliver dramatically improved results for laser systems, enhancing the experience for laser light show patrons.

Since light beams are only influenced by refraction, diffraction, or reflection, optical scanners have been developed to take advantage of each of these methods. So, in a broad sense, they can be classified as one of three types: acousto-optic scanners that deflect a beam using diffraction; electro-optic scanners that deflect a beam using refraction; and mechanical scanners (resonant, polygonal, and galvanometer scanning types) that deflect a beam using reflection. While all of these scanner types have been in use for decades, galvanometric scanners in the third group have significant benefits.

Acousto-optic and electro-optic scanners

With scanning speeds somewhat beyond 100 kHz, acousto- and electro-optic scanners can rapidly scan beams in random directions. However, their scan angle is typically limited to a few degrees or less, and often these scanners cannot be used with more than one wavelength simultaneously. The optical throughput of acousto-optic scanners is also limited to around 80% or less for a single axis, disqualifying them from laser light show venues.

Resonant and polygonal scanners

On the other hand, mechanical scanners work by rotating a physical mirror that can be coated to reflect any wavelength or combination of wavelengths with very high reflectivity—and thus, high optical throughput.

Using that physical mirror, both resonant and polygonal scanners can be made to scan a beam over very wide angles, but having the limitation of scanning the same pattern over and over again. For some applications such as printing, this is highly desirable, but for applications that require scanning of non-repeated patterns or positioning of a beam over a random area, the galvanometer scanner is the only choice.

Galvanometer scanners

Called galvos for short, mechanical galvanometer-based scanners involve a physical mirror operated by a motor of some kind. Most often, the mirror is attached to the shaft of the motor, but in some designs the mirror and motor may be a single integral unit.

Rather than simply spinning around, galvo motors are specialized and able to rotate over a limited range of angles (typically around ± 20°). Galvo motors also incorporate a high-precision position detector that provides feedback to a separate controller, delivering pointing repeatability of 5 μrad (5 mm at a distance of 1 km).

Galvos and virtually all mechanical scanners reflect the beam off of the

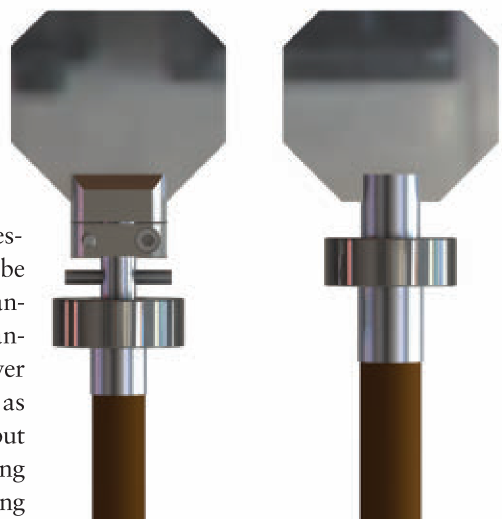

FIGURE 1. Conventional galvo rotor construction (left) is contrasted with ScannerMAX Saturn rotor construction (right).

rotating mirror such that the achievable scan angle in optical degrees is double the actual motor rotation angle. For galvos, this means that they can project beams up to 80° peak-to-peak or even more, and can be configured for two-axis scanning relatively easily.

Galvo limitations

For all of their benefits, including very wide scan angle, ability to scan multi-wavelength beams, high precision, and nearly 100% optical throughput, galvos do have a downside: speed. As mechanical scanners that impart real motion onto a physical mirror, galvos are limited by the laws of physics. Generally, this means that they have been relegated to scan frequencies between a few-hundred hertz and a few kilohertz.

And although physics can dictate how fast the physical mirror can be moved because of the force (torque) generated by the motor and the mass (inertia) of the mirror, it is not always obvious that other laws of physics dictate how fast the motor and mirror can be moved before being overcome by resonances. Very often, resonances in the system cause projected images to become distorted long before the motor has run out of the torque that could have produced greater scanning speeds.

Galvanometer evolution

A flurry of galvo scanner developments and patents started around 1976. These early designs involved the use of stationary Alnico magnets and "moving-iron" rotors. Indeed, moving-iron galvanometers had pretty good commercial success in strip-chart recorders, laser entertainment displays, and early laser marking machines.

Moving-iron galvos are generally hard-to-break, robust instruments. However, their relatively high electrical inductance and the magnetic circuit that allows the moving iron rotor to become saturated with magnetic flux places a hard upper limit on the amount of torque that can be developed. Although rotor stiffness (and thus the possibility to excite rotor and mirror resonance) is also lacking, moving-iron galvos were the tool of choice for around 20 years following their introduction.

Moving-coil galvos have also existed in one form or another for decades, with the earliest devices used in the 1900s. In the 1970s and 1980s, moving-coil galvos were also found in very specialized optical strip chart recorders, and throughout the 1990s were used in some laser marking machines. While still in use in specialized applications, they have never reached the degree of success of moving-iron galvos or of the next evolutionary step—the moving-magnet galvo.

Moving-magnet galvos

In 1992, galvo manufacturers started producing "moving-magnet scanners," so named because the rotor is made of a cylindrical magnet. Although moving magnet designs were conceived and patented in 1976, they were not practical until neodymium "super magnets" were developed in the late 1980s.

Because of the way the coil is formed inside the motor and where it is placed in the magnetic circuit, moving-magnet galvos have around 10X less electrical inductance than moving-iron galvos. Moreover, because there are no small, thin paths in the magnetic circuit, the magnetic saturation effects of moving-iron galvos are nonexistent, meaning that the laws of physics related to torque production are greatly alleviated—especially when short bursts of motion are used, as in laser marking applications.

Unfortunately, moving-magnet galvos do not solve all motor-related problems. When an application demands long periods of both high speed and wide-angle motion, the conventional moving-magnet motor construction is prone to overheating, as well as causing mirror flexing and resonance issues during scanning. And while advanced mirror materials such as silicon, silicon carbide, and beryllium can partially alleviate these resonance-related issues, access to these materials is limited and scanning system costs are increased while scanning speeds suffer.

A new formula

Frustrated by the stagnation in galvanometric scanning speeds, Pangolin president and chief engineer William R. Benner, Jr. began conceiving and developing scanners that would overcome the limitations of the conventional moving-magnet galvanometer. University professors who had written books on motor design as well as jet-airliner rotor design experts were brought in to analyze magnet/shaft/mirror interactions to identify the best possible combination of materials, shapes, and construction techniques.

After fine-tuning tens of thousands of design iterations in a computer using finite-element analysis techniques and building dozens of prototypes that resulted in a dozen patents with many of them already granted, Pangolin started a new division called ScannerMAX to manufacture its namesake galvo scanner.

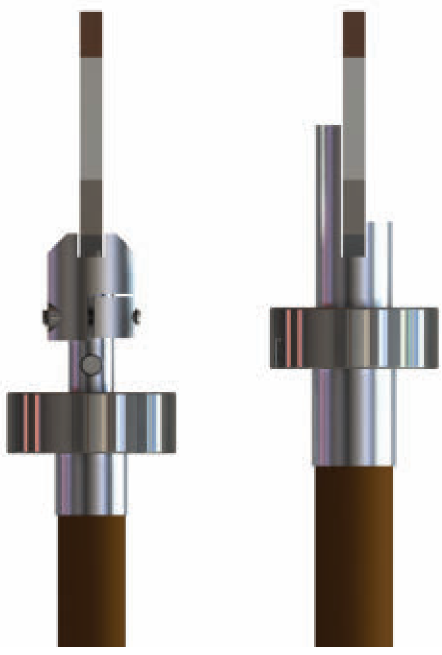

FIGURE 2. Conventional galvo rotor construction is shown with a cooler (left) vs. ScannerMAX Saturn rotor construction (right) that requires no cooling.

Essentially, these galvos are stronger and cooler, tackling two primary barriers that limit performance. First, as scanning speed is increased further and further, everything that rotates (the magnet, bearings, and any mirror mount) will become unstable, resulting in projected image distortion. And second, as more and more current is pumped into the galvo motor to produce more torque, heat is generated at a geometric rate. Since the motor can only take so much heat before destruction results, this places an upward limit on the amount of constant torque that can be produced by the motor.

Stronger galvos

Conventional galvos have an output shaft whose diameter is typically much smaller than the magnet. Manufacturers most often drill a hole through that small shaft, into which they place a "stopping pin" that limits the amount of motor rotation. Unfortunately, this means that the shaft must be made longer to accommodate the stopping pin, and is weakened by the hole accommodating the pin. A separate mirror mount is then used as an interface between the shaft and the mirror, thus adding to the distance between the magnet and the mirror.

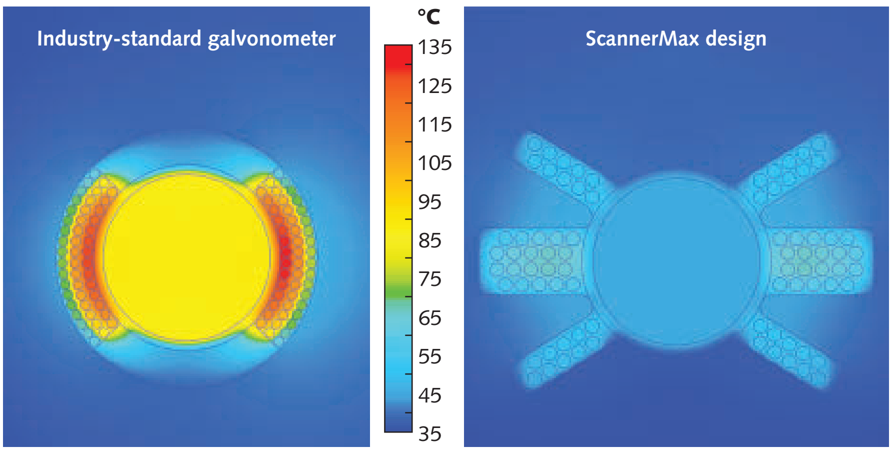

FIGURE 3. A conventional galvo motor is thermally overwhelmed (left) compared to a ScannerMAX Saturn motor (right) that exhibits much cooler operation while delivering the same torque.

In this case, the mirror mount typically only grips around 1 mm or less of the bottom edge of the mirror. With mirrors for scanning 10 mm laser beams being typically 24 mm long, this means that only 1/24th of the mirror is being supported by the mirror mount—a sub-optimal architecture that is fertile territory for resonances to occur. And although a notch filter is almost always needed in the servo driver to try to control the resonances, these filters also add phase delay in the servo loop and tend to affect the purity of the mirror motion.

The construction of ScannerMAX is different. The output shaft is typically the same diameter as that of the magnet, and since shaft stiffness is proportional to the fourth power of diameter, the stiffness increase based on diameter alone is more than 5X that of a conventional galvo. In addition, it uses no stopping pin and therefore needs no stopping hole, making the shaft as short as possible with no internal voids for maximum stiffness (see Fig. 1).

To limit motor rotation without a stopping hole, the scanner uses a patent-pending external mirror bumper. The mirror is then mounted directly into a slot in the shaft, so no separate mirror mount is used. Using this rotor technique, the distance between the magnet and the mirror (a factor that ultimately dictates resonances) is dramatically shorter.

Finally, the interface between the mirror and the shaft is not a simple slot, but rather one that includes a "back support." We liken this to the difference between sitting on a chair with a back and sitting on a barstool. The increased stiffness of all rotor components and improved mirror support system means that a notch filter is not needed in the servo loop, simplifying the servo design while also promoting very smooth and pure mirror motion.

Cooler galvos

Conventional galvos are constructed as a circular steel outer shell with copper wires placed between the steel and the concentric magnet. This leads to a variety of limitations, including the amount of flux density in the air gap because of the tradeoff between coil and air space, and the amount of heat that can be removed from the motor.

Alternatively, ScannerMAX uses copper wire between slots located within steel laminations in such a way that the air gap is significantly reduced and the flux density of the system is greatly increased (see Fig. 2). The slots also allow the use of thicker copper wire, lowering coil resistance.

With the increased flux density between the magnet and the steel, fewer turns of copper wire are needed to create the same amount of torque, allowing the motor to run much cooler than conventional galvos. These scanners are typically around 1/3 to 1/2 that of conventional galvos while delivering the same torque. And since heat in the galvo is directly proportional to coil resistance, they run much cooler for a given amount of torque production or, conversely, produce greater torque for a given amount of heat.

Increasing rotor stiffness increases scanning speeds by reducing system resonances, essentially staving off the frequency at which distorted images occur. Decreasing the coil resistance of the motor also increases scanning speeds by allowing the motor to operate at a higher speed before overheating. For laser light show displays, Pangolin's ScannerMAX Saturn 1 offers a scanning speed increase of 3X the industry standard and without external cooling (see Fig. 4).

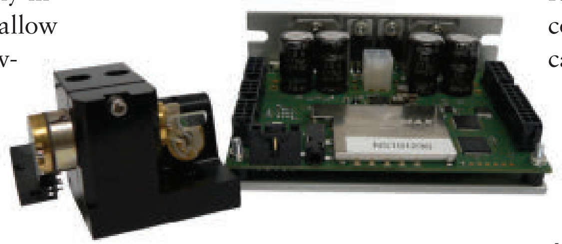

FIGURE 4. With speeds three times higher (and priced three times lower) than conventional galvo scanners, ScannerMAX requires less power, less physical space, and no external cooling.

In addition to projection displays, we believe the biggest beneficiary of this technology will be biomedical researchers performing confocal microscopy and optical coherence tomography since these applications have up to now depended on the current generation of conventional galvanometers that have a relatively short lifetime because of the heat produced during the scanning action.

Justin Perry is chief operating officer of Pangolin Laser Systems, Orlando, FL; e-mail: justin@pangolin.com; http://pangolin.com.

Tell us what you think about this article. Send an e-mail to LFWFeedback@pennwell.com.

BioOptics

NEWS & BREAKTHROUGHS

Technical advances in lasers, optics, and imaging for the life sciences

DNA SEQUENCING/FLUORESCENCE MICROSCOPY

Optical techniques help reveal schizophrenia's origins

A combination of optical techniques has helped researchers at the Broad Institute's Stanley Center for Psychiatric Research (Cambridge, MA), Harvard Medical School (Cambridge), and Boston Children's Hospital (Boston, MA) make a major genetic discovery that has important implications for future treatment of schizophrenia.[1]

Using droplet digital polymerese chain reaction (ddPCR, which incorporates flow cytometry) and two fluorescence imaging techniques (confocal microscopy and structured-illumination microscopy, or SIM), the researchers revealed that risk of schizophrenia increases in people who inherit specific variants of a gene related to synaptic pruning—that is, the elimination of connections between neurons.[2]

The study involved the collection of DNA from more than 100,000 people, detailed analysis of complex genetic variation in more than 65,000 human genomes, development of an innovative analytical strategy, examination of postmortem brain samples from hundreds of people, and the use of animal models to show that a protein from the immune system called C4 also plays a previously unsuspected role in the brain.

The findings show a causal link to schizophrenia. They also help explain that synaptic pruning is particularly active during adolescence (the typical period of onset for schizophrenia symptoms) and that the brains of patients with schizophrenia show fewer connections between neurons.

While therapies based on the work are years away, the findings raise the possibility that eventual treatments may be able to minimize synaptic pruning in individuals who show early symptoms of the disorder. This would enable a dramatically different approach from current therapies that address only the psychosis associated with schizophrenia and do not treat other symptoms, including cognitive decline.

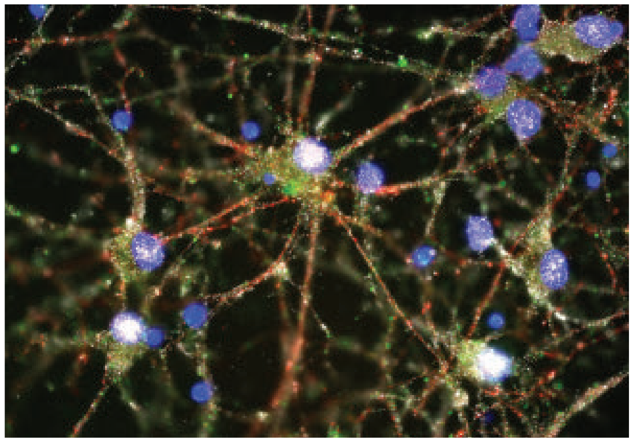

Imaging studies found C4 (green) at synapses (red and white) of cultured human neurons (blue). *(Image courtesy of Heather de Rivera, McCarroll lab)*

1. A. Sekar et al., *Nature*, 530, 177–183 (2016).
2. ddPCR is a trademark of Bio-Rad Laboratories, Inc.

NEUROSURGERY/LASER THERAPY

Laser opens blood-brain barrier for chemotherapy

Laser technology was FDA-approved for surgical treatment of brain tumors in 2009. Now, new research demonstrates the ability of 1064 nm laser light to disrupt the blood-brain barrier, which protects the brain from toxins and has limited treatment options for brain cancer patients.[1]

In a pilot study of minimally invasive laser surgery for glioblastoma (the most common and aggressive type of brain cancer), researchers at Washington University School of Medicine in St. Louis (MO) unexpectedly found that MRI-guided laser interstitial thermal therapy (LITT) enabled permeability of the blood-brain barrier for up to six weeks—long enough for patients to receive multiple chemotherapy treatments. Because the opening in the protective layer can be confined to a spot near the tumor, the blood-brain barrier remains intact elsewhere—potentially limiting harmful effects of chemotherapy to other areas of the brain, the researchers said.

As part of the trial, 13 patients received doxorubicin intravenously in the weeks following surgery with the NeuroBlate laser ablation system (Monteris Medical). The researchers are closely following the participants, said Professor of Neurosurgery Eric C. Leuthardt, MD. "Our early results indicate that the patients are doing much better on average, in terms of survival and clinical outcomes, than what we would expect. We are encouraged but very cautious because additional patients need to be evaluated before we can draw firm conclusions."

Other successful attempts to breach the barrier have left it open for only about 24 hours (not long enough for consistent chemotherapy) or have produced limited benefit. The new findings may enable the application of other treatments, such as cancer immunotherapy, which harnesses cells of the immune system to locate and destroy cancerous tissue.

The pilot study is part of a phase II clinical trial that will involve 40 patients. The researchers are also planning another clinical trial combining the laser technology with chemotherapy and immunotherapy, as well as trials to test targeted cancer drugs that normally can't breach the blood-brain barrier.

Washington University neurosurgeon Eric C. Leuthardt, MD, is lead author on a paper describing a newly discovered benefit of laser surgery for patients with glioblastomas. *(Photo courtesy of Robert Boston/ School of Medicine)*

1. E. C. Leuthardt et al., *PLoS One*, 11, 2, e0148613 (2016).

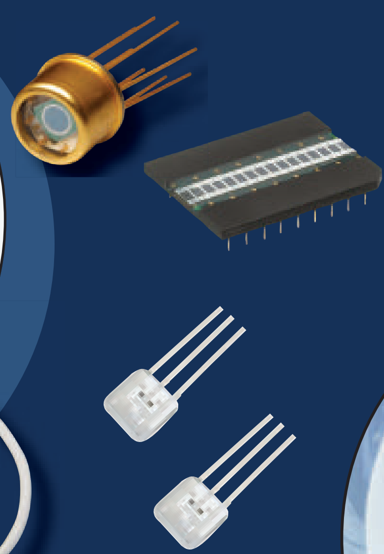

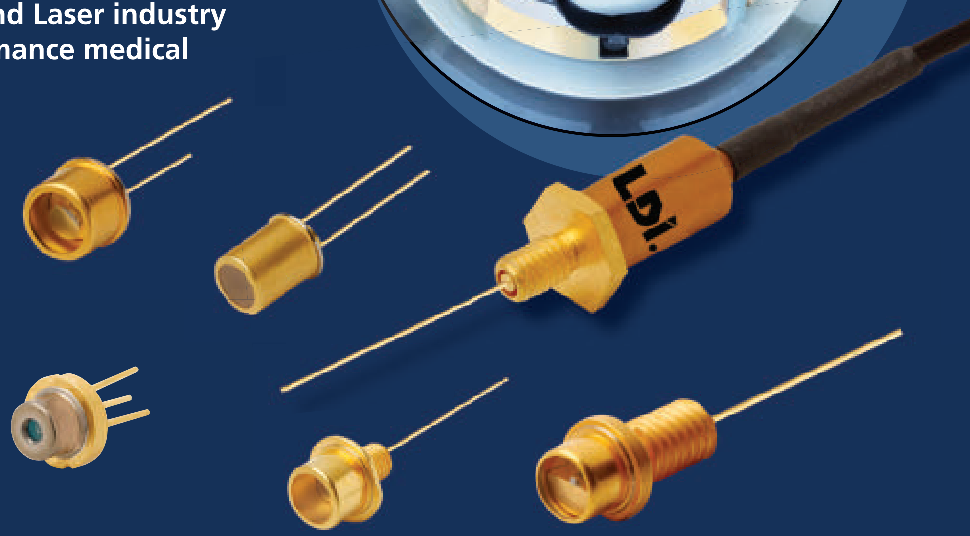
LDI.

A new optical window opens for deep brain imaging

LINGYAN SHI

New research demonstrates that near-infrared (NIR) light in the 1600–1870 nm range is optimal for imaging of brain tissue, surpassing the traditional "therapeutic window" for light transmission and decreased absorbance. This "golden window" has been discovered by the availability of new tools, including femtosecond lasers and photodetectors based on indium gallium arsenide (InGaAs) or indium antimonide (InSb).

Optical imaging is critical to life sciences because it enables superior spatial resolution. But because scattering and absorption are inherent barriers to light propagation in tissue (scattering blurs images while absorption reduces availability of photons), a key goal is maximizing optical imaging depth. This is true for bioimaging in general, and neuroimaging in particular.

Because the scattering coefficient decreases with increasing wavelength, light of longer wavelengths is able to penetrate deeper into tissue. Compared with wavelengths in the visible range, near-infrared (NIR) light at 650–950 nm—commonly known as the "therapeutic window," and what we call Optical Window 1—has been recognized as advantageous for its reduced absorption and scattering. The availability of low band gap silicon-based photodetectors has enabled scientists in recent years to leverage these advantages for deep-tissue imaging. But while technology has limited access to wavelengths beyond 950 nm, new advances—specifically suitable detectors and femtosecond laser sources—offer greater potential. Such tools have facilitated research, revealing three additional NIR optical windows and corresponding facilitation of deeper imaging. New work shows the promise of one window in particular for optimal imaging of brain tissue.[1] The work examined the transmission of light through brain tissue, and applied theoretical study to estimate optical parameters and determine the key wavelengths and attenuation coefficients in four NIR ranges.

Using the tools

When propagating through tissue, light separates into ballistic, snake, and diffusive components.[2,3] Multiphoton microscopy enables deep-tissue imaging by using the ballistic component of NIR light to excite fluorescence in Optical Window 1. Exciting fluorescent agents to their second singlet (S2) state, where both the excitation and emission wavelengths fall within the optical window, enables deeper imaging.[4] The difficulty of the S2 pumping technique lies in a dearth of appropriate contrast agents. An alternate solution is to apply longer NIR wavelengths for tissue imaging, so that—in line with Rayleigh and Mie theories—scattering and absorption are further decreased.

Researchers at City University New York reported imaging of tissues in three longer-wavelength NIR regions:

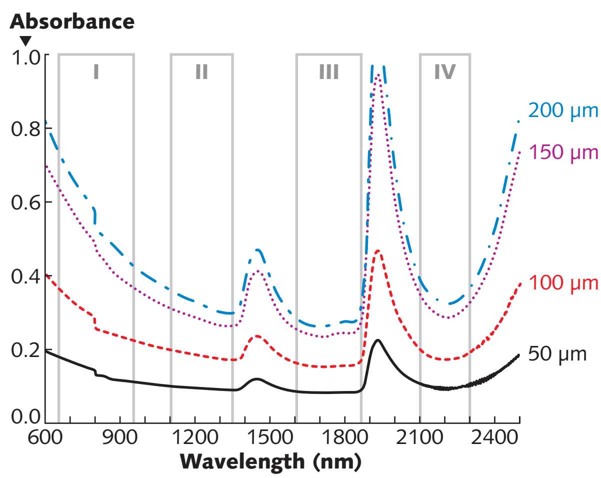

Measuring absorbance in the four tissue thicknesses (50, 100, 150, and 200 μm) using optical tissue windows I, II, III and IV revealed a trough of absorbance spectra in Window III, the "Golden Window," (1600–1870 nm). *(Adapted from L. Shi, L. A. Sordillo, A. Rodríguez-Contreras, and R. Alfano[1])*

Optical Window II (1100–1350 nm), Window III (1600–1870 nm), and Window IV (centered at 2200 nm).[5] Even more recent work investigated key properties of light in the three windows compared with the traditional therapeutic window. It calculated corresponding attenuation length (lt) using rat brain sliced at four different thicknesses (50, 100, 150, and 200 μm). Using a UV/VIS/NIR spectrophotometer that measured light transmission through each slice, we were able to identify the optical window with the lowest scattering and noise, and optimized absorption—that is, the window best suited for imaging brain tissue.

Peak transmittance T (%) of brain tissues measured in each optical window

Window	Tissue thickness			
	50 μm	100 μm	150 μm	200 μm
I	77.3	59.8	43.0	37.4
II	81.5	67.5	54.5	50.4
III	82.9	70.5	58.1	54.6
IV	81.0	67.7	51.7	47.8

Transmittance and absorbance

A study of peak transmittance for the 50, 100, 150, and 200 μm slices in the various wavelength ranges (summarized in the table) demonstrates that all three of the "new" optical windows enable deeper imaging than the standard therapeutic window of 650–950 nm. And it shows that Window III (1600–1870 nm) is best at facilitating peak transmittance. Window III turns out to be best in terms of absorption as well: Looking at measured absorbance of light through the four tissue thicknesses in the various windows reveals a trough of absorbance spectra in that range (see figure). For these reasons, we call Window III the Golden Window for brain imaging.

The ballistic photons in scattering media are governed by the Beer-Lambert law, which can be adjusted to incorporate diffusive mode. We used this equation to evaluate the role that each mode plays in light transmission through brain tissue: We performed simulations in the four optical windows and compared the results with our peak transmittance measurements. The model simulation results matched well with our experimental results across the board. The results also suggested that ballistic mode played a dominant role in our experiment, and that the role diffusive mode played is minimal.

Other studies examining Window III have confirmed its value. The work at City College New York comparing all four NIR optical windows also found Window III to be optimal for imaging.[5] Scientists at Purdue University (West Lafayette, IN) demonstrated that Window III allows deeper tissue penetration in their study of overtones and combination modes in the methyl groups of proteins, amino acids, and lipids.[6] And work by InfraReDx Inc. (Burlington, MA) suggests that Window III is optimal for exploring the cholesterol and collagen content of different types of tissue.[7]

Brain tissue is distinct from other tissue types. Compared with muscle, for instance, it contains twice as much lipid, but less than half as much protein.[8] More work is needed to determine the impact of these and other tissue components on optimal wavelength, and to compare neural and other tissues. This work promises to facilitate imaging of brain tissue in space. New CMOS cameras and photodetectors based on InSb will also help to improve imaging of blood vessels within the brain, and extracellular space, *in vivo*. We look forward to further work advanced by these tools.

REFERENCES

1. L. Shi, L. A. Sordillo, A. Rodríguez-Contreras, and R. Alfano, *J. Biophoton.*, 9, 1–2, 38–43 (2016).
2. L. Wang, P. P. Ho, C. Liu, G. Zhang, and R. R. Alfano, *Science*, 253, 769–771 (1991).
3. R. R. Alfano, W. B. Wang, L. Wang, and S. K. Gayen, *PHOTONICS: Scientific Foundations, Technology and Applications* (ed. D. L. Andrews), John Wiley & Sons, Hoboken, NJ (2015).
4. L. Shi et al., *J. Biomed. Opt.*, 19, 066009 (2014).
5. L. A. Sordillo, Y. Pu, S. Pratavieira, Y. Budansky, and R. R. Alfano, *J. Biomed. Opt.*, 19, 056004 (2014).
6. P. Wang, H. W. Wang, M. Sturek, and J. X. Cheng, *J. Biophoton.*, 5, 25–32 (2012).
7. J. D. Caplan, S. Waxman, R. W. Nesto, and J. E. Muller, *J. Am. Coll. Cardiol.*, 47, C92–C96 (2006).
8. H. McIlwain and H. S. Bachelard, *Biochemistry and the central nervous system*, Churchill Livingstone, New York (1985).

Lingyan Shi *is a research associate at the Institute for Ultrafast Spectroscopy and Lasers and Biology Department at City College of the City University of New York, New York, NY; e-mail: lshi365@gmail.com; www.ccny.cuny.edu/iusl.*

Melanoma detection with SWIR Raman spectroscopy

PETER J. CASPERS, PATRICK MERKEN, RAF VANDERSMISSEN, INES SANTOS, and **GERWIN PUPPELS**

Low readout noise—enabled by advanced detector technology—has facilitated the development of a technique for applying shortwave-infrared spectroscopy to the examination of darkly pigmented tissue. The nondestructive, noncontact approach suppresses spectral disturbance to greatly facilitate the diagnosis of melanoma.

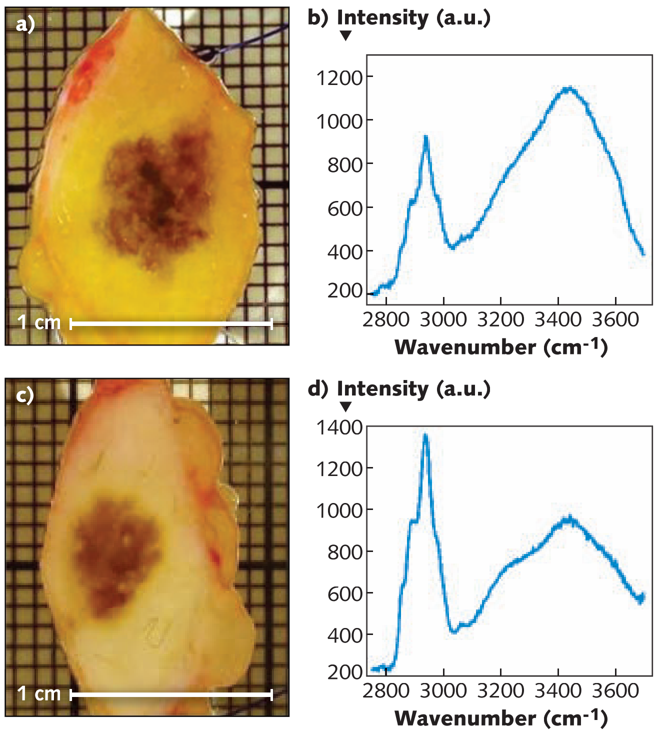

Photographs and Raman spectra obtained with the experimental setup of pigmented human tissue indicating melanoma (a, b) and benign melanocytic tissue (b, c). Laser wavelength: 976 nm, exposure time: 10 s. (*From I. P. Santos et al.*[1])

"Raman spectroscopy is a very versatile technique to look at anything that you can shine light on," says Gerwin J. Puppels. Puppels is is founder of spectroscopy systems developer RiverD International B.V. (Rotterdam, The Netherlands) and one of six researchers at the Erasmus University Medical Center (Rotterdam, The Netherlands) who collaborated with RiverD International on an extensive project funded by the Netherlands Ministry of Economic Affairs to explore medical application of Raman spectroscopy.[1] What makes the technique attractive for biomedicine is its power, sensitivity, and ability to deliver high-resolution quantitative analysis without destructive effect on—or even contact with—specimens.

Raman spectroscopy measures the inelastic scattering of light from the molecules of a specimen illuminated at low levels by monochromatic light from a laser or other source. The sample absorbs photons from the illuminating light source and re-emits them with a slightly shifted (up or down) frequency. The downshifted frequency, used in the application of the Raman effect, is called the Stokes frequency—its upwards-shifted counterpart is called "anti-Stokes." Stokes and anti-Stokes frequency parts represent a minuscule fraction of 0.001% of the total light reflected by the sample because of elastic scattering called Rayleigh scattering.

Separating the weak desired Stokes frequency part from the extremely energetic Rayleigh scattering requires an elaborate setup of apertures, filters, or multi-spectroscopic and tuning devices. To overcome these difficulties, various methods have been conceived and developed for sample illumination and detection. Among these methods are stimulated irradiation, coherent anti-Stokes or nonlinear stimulation, and surface-enhanced Raman spectroscopy (SERS) using signal emission from metallic surfaces. Thus, despite its inherent difficulties, researchers have successfully developed Raman spectroscopy for numerous applications.

The detector of choice for Raman spectroscopy has been a silicon-based

CCD sensor. But the fact that usable responsivity range of a CCD tops out at 1 μm is a serious limitation for medical applications, especially for investigating and characterizing darkly pigmented tissue. In the visible spectrum, such specimens emit strong fluorescence, which severely impacts the obtained Raman spectra.

While researchers have made numerous attempts to mitigate analytical degradation by fluorescence—for example, with time-gated detection, photobleaching, confocal signal detection, SERS, and resonance Raman (RR) scattering—none have led to a suitable setup for *in vivo* Raman spectroscopy of pigmented tissues. Fourier-transform (FT) Raman spectroscopy, however, has demonstrated the ability to yield usable spectra of pigmented skin lesions.[1] FT Raman proves that tissue fluorescence can be successfully sidetracked by deploying a longer laser excitation wavelength—for example, 1064 nm. For these reasons, the Erasmus researchers found FT Raman compelling, but they ultimately had to reject the technique. Because it is based on the multiplexing of single-channel analysis, FT Raman's signal integration times can exceed those of multichannel Raman spectroscopy by several orders of magnitude (it requires one to tens of minutes to investigate results in a single spectrum). "It provides nice scientific results, but is hardly usable in medical practice," Puppels says.

Raman in the SWIR

So, the team needed to take a different path. And there, they encountered another hurdle.

Thanks to the extremely weak intensity of the Raman signal, Raman spectroscopy's main limitation is noise floor—which is exaggerated when the detector adds readout noise. "If you observe a signal—say, 10,000 photons—the shot noise on the signal is 100 photons," explains Puppels. "This would give you a signal-to-noise ratio of 100. Unfortunately, the readout noise of the detector will typically add an additional several hundreds of electrons, and the Raman measurement is no longer shot noise-limited. That puts you in a very bad position—especially when encountering weak signals consisting of just 10,000 photons."

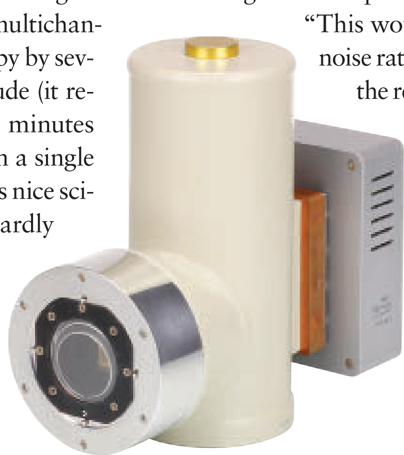

FIGURE 1. The Xenics Cougar camera contains an InGaAs focal plane detector suited for image capture in the shortwave-infrared (SWIR).

While CCD detectors typically add 2–3 electrons of noise, InGaAs cameras operable beyond 1 μm have traditionally delivered readout noise of up to several hundred electrons. The team needed a detector capable of reaching beyond 1 μm, but adding minimal noise.

They found their solution in a camera that had never been used for medical spectroscopy—a high-performance camera designed for extreme low-light-level imaging applications in the shortwave-infrared (SWIR) realm, and for such demanding applications as photoluminescence measurements in semiconductor manufacturing and failure analysis. Investigating the camera, the researchers found Raman spectroscopy listed among its applications. Puppels was intrigued. “This might be a very promising avenue opening up to collect the Raman spectrum in seconds instead of minutes and hours,” he said.

The Xenics (Leuven, Belgium) Cougar-640 (see Fig. 1) incorporates an InGaAs focal plane array detector (XFPA-1.7-640-LN2) featuring 640 × 512 pixels (at a pixel pitch of 20 μm) and a 24-bit analog-to-digital converter (ADC). A source follower per detector (SFD) readout scheme enables ultra-low noise levels (to <20 e-). Each pixel features a full-well capacity of about 480,000 electrons, and a conversion gain of 2.17 μV/e-. Typical dark current is <20 e-/sec/pixel, at 77K sensor temperature and with a target emissivity of 5% and target temperature at 300K. Even lower dark current values are achievable with a liquid nitrogen (LN_2)-cooled target (~77K).

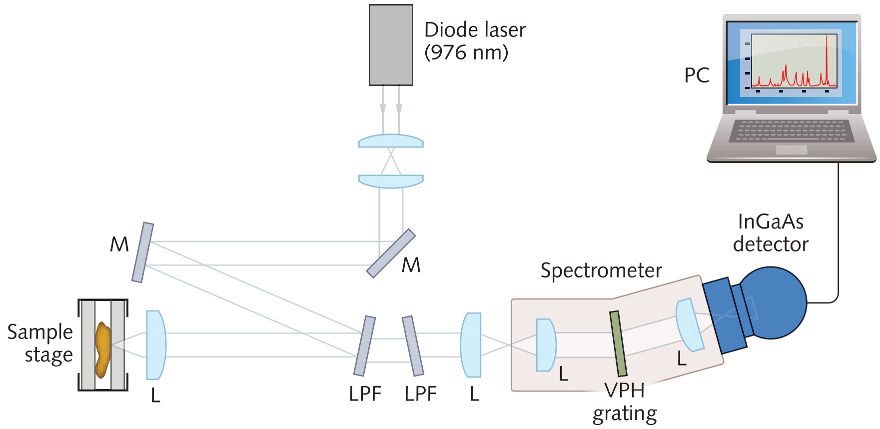

FIGURE 2. The experimental setup used in the Erasmus University Medical Research Center Rotterdam research has demonstrated that Raman spectroscopy can be successfully used in medical practice, delivering high-quality, high-wavenumber (HWVN) Raman spectra with a low fluorescence background. (*From I. P. Santos et al.*[1])

To demonstrate the feasibility of wavelength-shifted Raman spectroscopy, the team devised and built a complete SWIR multichannel instrument that included the camera (see Fig. 2). For a light source, they used a single-mode continuous-wave diode laser radiating at 976 nm—which provided output power of 150 mW (Model R-type from Innovative Photonic Solutions [Monmouth Junction, NJ]).

Adjusting for medical applications

A key point of interest was the fact that the camera's readout scheme—called Read While Integrate (RWI)—enables lowering read noise by an order of magnitude. RWI, sometimes called "up-the-ramp readout," probes the accumulating photoelectrons through nondestructive sampling without resetting the buffering capacitors. The approach enables operation of the camera in extremely low-light-level applications, and it virtually eliminates effective readout noise.

Because the camera had never been used for medical spectroscopy, the team determined to enhance some of its characteristics by developing software to augment that supplied by Xenics. They wrote algorithms to read and pre-process the raw data that is delivered in the camera's RWI readout scheme.

Also, the camera's response curve showed a definite progressive nonlinear behavior when the accumulated signal exceeded a certain threshold, which necessitated a cutoff threshold for a more linear behavior. So, they devised an algorithm to correct the response above the threshold—for this purpose, they fitted a first-order polynomial to the linear range during the first part of the integration period. The frontis image (see p. 58) shows some tissue samples obtained with the experimental SWIR Raman spectroscopy setup.

The RWI principle was devised for industrial applications such as inspecting semiconductor chips for leakage. Such measurement takes time while the signal builds up.

The Erasmus team's software operates similarly, nondestructively capturing the signal many times before producing a final averaged result. The effective noise level can be very low. The team reports having reduced from ~20 to ~2 e-, effectively.

The team found the detector's readout noise (in e-, with CDS) to be 22.7 e- (with 5.9 e- standard deviation), and dark current (e-/s/pixel) at 69.4 e-/s/pixel (with 4.5 e-/s/pixel standard deviation). Note that dark current strongly depends on target temperature and target emissivity. This noise level substantially decreases with more sampling readouts during the

Effective readout noise levels obtained with the InGaAs detector of the Cougar camera

Number of intermediate readouts	Effective readout noise (e-/pixel)
2	16.2
100	2.27

[*SOURCE: I. P. Santos et al.*[1]]

integration time. The final results given in the table (see p. 61) indicate that the effective readout noise was reduced to the value comparable to cooled slow-scan CCD detectors.

The researchers caution that there are technical challenges yet to overcome. Raman spectroscopy's low signal-to-noise ratio implies limits for performing in the SWIR range to circumvent fluorescence effects produced by pigmented tissue in the visible realm. Not the least of these is cost. But an array with fewer pixels may be sufficient for medical applications, and such adjustments will be the focus of future work. In any case, this work is expected to substantially further the diagnosis of melanoma.

REFERENCE

1. I. P. Santos et al., *J. Raman Spectrosc.*, doi:10.1002/jrs.4714 (2015).

Peter J. Caspers, *Ph.D., is a researcher at Erasmus University Medical Center, Rotterdam, The Netherlands;* **Patrick Merken** *is CTO at Xenics, Leuven, Belgium;* **Raf Vandersmissen** *is CEO of sInfraRed Pte Ltd. – a Xenics company, Midview City, Singapore;* **Ines Santos** *is a PhD student at Erasmus University Medical Center; and* **Gerwin Puppels** *is founder of RiverD International, Rotterdam, The Netherlands; e-mail: p.caspers@erasmusmc.nl; www.erasmusmc.nl.*

New products

Would you like to be included? Please send your product description with high-resolution digital image to: lfwnewproducts@pennwell.com

Automatic bias controller

The IQABC automatic bias controller (ABC) controls and optimizes all modulator bias points, regardless of the modulation format or pattern. Six Mach-Zehnder bias control channels inside one dual-polarization IQ modulator simultaneously influence the properties of a single optical signal.

Coherent Solutions
Rosedale, Auckland, New Zealand
www.coherent-solutions.com

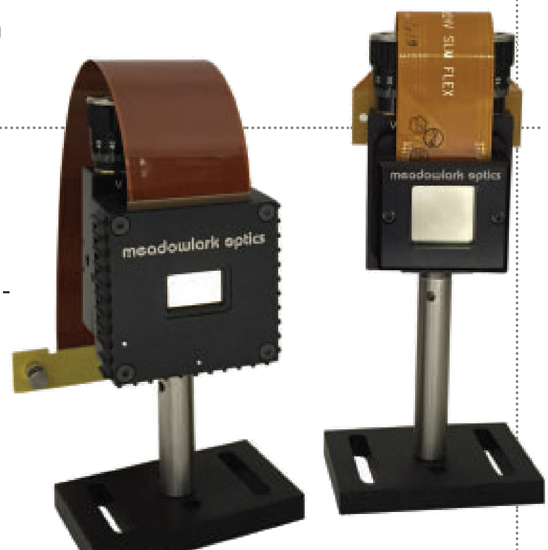

Analog spatial light modulators

Two analog spatial light modulators (SLMs) work to control incident light in amplitude, phase, or a combination of both on a pixel-by-pixel basis for computer-generated holography. The 1920 × 1152 SLM provides 12 bits of phase control at each pixel, and the 512 × 512 version offers larger pixels and additional optical shielding for use in high-power laser applications.

Meadowlark Optics
Frederick, CO
www.meadowlark.com

CW/pulsed mid-IR laser

The Hedgehog rapid-scan continuous-wave (CW)/pulsed laser can tune up to 400 cm^{-1} at >1000 cm^{-1}/s. Average or

peak powers are up to 400 mW, and it includes a SideKick multi-function QCL controller. Optimized for mid-infrared (MIR) spectroscopy, with a small, sealed head, it is intended for OEM integration or lab use.

Daylight Solutions
San Diego, CA
www.daylightsolutions.com

Micro-patterned filters

Micro-patterned optical coatings com-

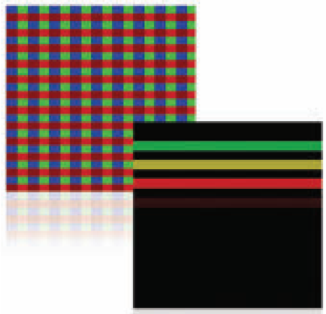

bine patented microlithography techniques with state-of-the-art coating technology. This allows patterning of multiple dielectric, metal, and color gel filter array coatings on a single substrate. Standardized processes are in place for patterning on glass and semiconductor wafers.

PIXELTEQ
Largo, FL
www.pixelteq.com

IR array thermal imager

The MLX90621 infrared array delivers an expanded field of view at 30 × 120° to measure temperature profiles of both passenger and driver from a single position on the dashboard center-stack. It offers a programmable frame rate of 0.5 to 512 Hz, and is available in a TO-39

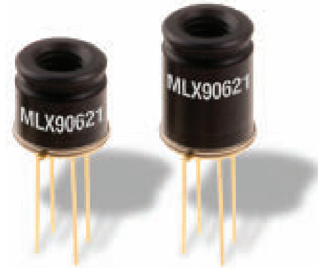

metal can package for a 16 × 4 pixel thermal array.

Digi-Key
Thief River Falls, MN
www.digikey.com

XY motion platform

The CXY-BS Series 150 mm precision XY motion platform exhibits orthogonality of 10 arcsec to enable 150 mm of XY

travel with 10 μm linear accuracy and 1 μm linear repeatability. The compact, low-profile, ball-screw drive stage is suited for microscopy, inspection, wafer processing, laser marking, and optical positioning.

Griffin Motion
Apex, NC
www.griffinmotion.com

Terahertz measurement kits

The Air-Coupled Measurement Kit and Fiber-Coupled Measurement Kit provide

customizable solutions for research labs and post-secondary classrooms. The fiber-coupled kit allows advanced optics labs to demonstrate terahertz and optical measurements to students, while the air-coupled kit allows users to build terahertz time-domain setups.

TeTechS
Waterloo, ON, Canada
www.techs.com

Epoxy gel system

Super Gel 9 is a two-component, urethane modified epoxy system that cures at room temperature to form a soft, resilient, gel-like system. This optically

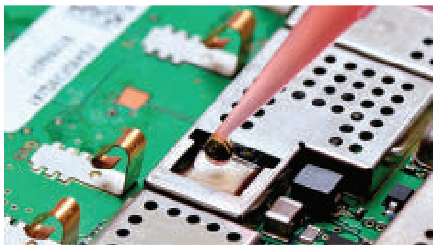

clear system has low hardness of ~5–10 Shore A. It can be cast in sections up to 2–3 in. thick and is suited for potting/encapsulation electronic parts and optical components.

Master Bond
Hackensack, NJ
www.masterbond.com

Simulation software

Part of the Multiphysics version 5.2 simulation software, LiveLink for SOLIDWORKS connects software simulations and 3D design and allows users to build apps with the applications builder. Users can import and perform operations on their CAD geometries from within an app and then synchronize the final geometry with SOLIDWORKS software.

COMSOL
Burlington, MA
www.comsol.com

Manufacturers' Product Showcase

Measure Laser Power Down to 300fW

Ophir Photonics Group, a Newport Corporation company celebrating 40 years of excellence as the global leader in precision laser measurement equipment introduces the **RM9-PD Radiometer**, a sensor for measuring the power of very low level CW or quasi CW sources. The sensor is calibrated over the entire range of wavelengths, from 0.2μm to 1.1μm, and features reduced external noise; allowing the sensor to measure power levels from 300fW to 300nW.

OPHIR® Photonics — A Newport Company
Spiricon® OPHIR Photonics — A Newport Company

sales@us.ophiropt.com • +1 435-753-3729
www.ophiropt.com/photonics

WM-1210 Wavemeter

New Focus, a Newport Company and leader in photonics solutions, is introducing its first Wavemeter, the WM-1210. This easy-to-use instrument requires minimal setup and provides optical wavelength measurements in the 700–1650 wavelength range with ±1 ppm accuracy. The front panel display makes reading measurements simple and straightforward.

New Focus™ — A Newport Company

New Focus, A Newport Company
(800) 222-6440
www.newport.com/newfocus

Agility™ Dual-band Transportable Raman Analyzer

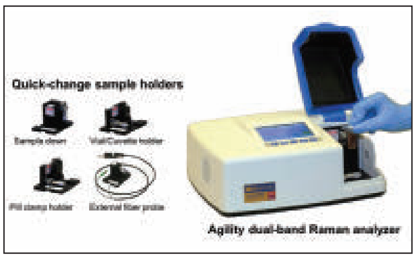

BaySpec's *Agility*™ Raman analyzer delivers high sensitivity, reliability and mobility in an affordable, ruggedized, battery-operated turn-key package. The dual-band configuration (any two laser excitations of 532, 785, and 1064 nm with automatic laser switch) significantly increases successful measurement rate, with single-band affordability. The dual excitation option maximizes selectivity for almost all real-world samples with speed, sensitivity and fluorescence rejection by 1064-nm laser Raman. Quick-change, auto-aligning sample holders make sampling flexible. Powerful software allows users to easily view and process spectra, verify sample identification and configure user spectral libraries, while providing FDA 21 CFR Part 11 compliance.

BAYSPEC
Pervasive Spectroscopy

www.bayspec.com • sales@bayspec.com

Manufacturers' Product Showcase

HVM 2-in. OEM Vertical Drive Mirror Mount

Newport's HVM-1i mirror mounts set the standard for OEM vertical-drive mirror mounts. Now, this exceptional mount is available in a 2-inch version with hex-key adjusters and locks. We call it the HVM-2i. All of the great performance features of the original HVM-1i are carried on: angular range of +/- 3.5°, high-precision 80-TP fine adjustment screws and patented, built-in locks. Also available as the M-HVM-2i with M4 metric mounting threads.

Newport
Experience | Solutions

(800) 222-6440
www.newport.com
sales@newport.com

Low-Distortion Suprema™ Mirror Mounts

The new Low-Distortion Suprema Mirror Mounts offer the combination of low optical distortion and outstanding long-term stability. Each mount has a unique low-stress faceplate to mount the optic. This mounting feature reduces wave front distortion by over 70% compared to standard set screw retained optics. All Suprema mirror mounts have stainless steel bodies and precision carbide kinematic pads to ensure low thermal drift making them ideal for applications in laser instruments and research.

Newport
Experience | Solutions

(800) 222-6440
www.newport.com
sales@newport.com

40 – 500 ps Rise Time Pulse Generators and Laser Diode Drivers

Avtech has pioneered the design of subnanosecond rise time pulse generators and drivers and now offers over 60 models which provide 40-500 ps rise times with 5 to 100 Volt output amplitude and PRF to 200 MHz. These models are ideal for testing high speed semi-conductors and opto-electronics in both laboratory and factory floor applications. Customized models are also available.

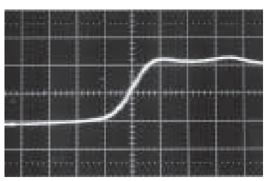

50 ps/DIV, 5V/DIV
Model AVP-3SA-C

And Model AVI-V-HV2A-B provides a 100 Volt, 300 ps rise time output!

AVTECH

Pricing, manuals, datasheets and test results at
http://www.avtechpulse.com/laser
More information: info@avtechpulse.com

LaserFocusWorld® ONLINE

www.laserfocusworld.com

PennWell®

Manufacturers’ Product Showcase

Advertiser index

This ad index is published as a service. The publisher does not assume any liability for errors or omissions.
Send all orders & ad materials to: Ad Services Specialist, Laser Focus World, 1421 S. Sheridan, Tulsa OK 74112

LaserFocusWorld®

ADVERTISING SALES OFFICES

MAIN OFFICE

61 Spit Brook Road, Suite 401, Nashua, NH 03060
(603) 891-0123; fax (603) 891-0574

Publisher
Alan Bergstein
(603) 891-9447; alanb@pennwell.com

Executive Sales and Marketing Assistant
Julia Campbell
(603) 891-9174; juliac@pennwell.com

Digital Media Sales Operations Manager
Tom Markley
(603) 891-9307; thomasm@pennwell.com

Ad Services Manager
Alison Boyer-Murray
(918) 832-9369; fax (918) 831-9153
alisonb@pennwell.com

Director, List Sales
Kelli Berry
(918) 831-9782; kellib@pennwell.com

NORTH AMERICA

North America: East & Central
Jeff Nichols, National Sales Manager
(413) 442-2526; fax (413) 442-2527
jeffn@pennwell.com

North America: West & Mountain
AnneMarie St. John-Brooks,
(510) 606-0630; annemarie@pennwell.com

INTERNATIONAL

Austria, France, Germany, Switzerland, Russian Federation, United Kingdom
Holger Gerisch
+49-(0)8801-9153791; fax +49-(0)8801-9153792
holgerg@pennwell.com

Hong Kong/China Adonis Mak
852-2-838-6298; fax 852-2-838-2766
adonism@actintl.com.hk

India Rajan Sharma
91-11-686-1113; fax 91-11-686-1112
rajan@interadsindia.com

Israel (Tel Aviv) Dan Aronovic
972-9-899-5813; aronovic@actcom.co.il

Japan Masaki Mori
81-3-6721-9890; masaki.mori@ex-press.jp

Taiwan Diana Wei
886-2-2396-5128 ext. 270; fax: 886-2-2396-7816
diana@arco.com.tw

For all other international sales, please contact: Alan Bergstein, Publisher (see contact info. above)

For assistance with marketing strategy or ad creation, please contact:

Marketing Solutions
Vice President Paul Andrews
240.595.2352
pandrews@pennwell.com

Laser Focus World® (ISSN 1043-8092), Volume 52, No. 3. *Laser Focus World* is published 12 times a year, monthly by PennWell® Corporation, 1421 S. Sheridan, Tulsa, OK 74112. Periodicals postage paid at Tulsa, OK 74112 and at additional mailing offices. **SUBSCRIPTION PRICES:** USA $162 1yr., $310 2 yr., $443 3 yr.; Canada $216 1 yr., $369 2 yr., $507 3 yr.; International $270 1 yr., $435 2 yr., $578 3 yr. **POSTMASTER:** Send address corrections to *Laser Focus World*, P.O. Box 3425, Northbrook, IL 60065-3425. Laser Focus World is a registered trademark.

Printed in the USA. GST No. 126813153. Publications Mail Agreement no. 40052420.

Industrial laser markets in China—changing and still growing

MILTON CHANG

I attended the 2016 Lasers & Photonics Marketplace Seminar in San Francisco and found it very informative. Here, I will summarize what I have learned from Dr. Bo Gu in his informative speech titled "The Changing Laser Market in China," to which I have added my own commentary, with his review.

Bo worked for IPG Photonics as Director of Asian Operations and General Manager of IPG China from 2008 to 2012 before he formed BOS Photonics to develop photonics technologies and provide consulting services. A Fellow of OSA and SPIE, he is currently on the Executive Committee of the Chinese Optical Society and vice president of its Laser Processing Committee.

Bo presented his take on the Chinese economy and also a comprehensive report on the sale of industrial lasers in China. As you can imagine, application is pervasive in the manufacturing of cell phones, automotive parts, oil/gas pipelines, high-speed trains, etc. And laser 3D manufacturing has been proclaimed a national priority. The trend is toward the purchase of complete automated systems, including visual detection, automatic feeding, blanking, auto cleaning, inspection, and classification. OEM manufacturers are now consolidating to become more vertically integrated, and there are many mergers and acquisitions in the midst of an economic slowdown.

A significant number of industrial fiber lasers are now manufactured by domestic companies—70% in the low-power range to 50% in the mid-power range—and the number is expected to increase from the current 5% for high-power fiber lasers. There is also significant price erosion: a marking system that used to cost $30,000 in 2011 is currently $7000 and expected to drop to $3000 in 2016, and a 3 W fiber laser that cost $70,000 in 2011 is now $22,000. Total revenue remains constant for laser companies compensated for by higher unit volume, but that implies significantly shrinking profit margins.

Dr. Bo Gu

Bo provided a balanced view of the economic situation in China—the bad news is pretty much in line with what we have read in the press here. But the impression I walked away with is the economy in China is in reasonable shape: 13.7 million jobs created with 4.2% unemployment in 2015 compared to 2.7 million jobs and 5% unemployment in the U.S., as well as 7 million college graduates mostly in technical fields compared to 1.8 million in the U.S. mostly in nontechnical fields. Also, the central government is planning to increase the urban population from 56% to 70% by 2030, which will stimulate the economy because of the construction of housing and infrastructure. When we compare statistics in China with statistics in the U.S., we have to keep in mind that China has more than four times the U.S. population (1.357 billion vs. 318 million).

What really deserves our attention is the national initiatives, such as the Made in China 2025 initiative to "comprehensively upgrade" Chinese industry. Reacting to U.S. advanced manufacturing programs, this initiative is also inspired by Germany's Industrie 4.0 plan, and there is considerable exchange between the two countries to their mutual benefit.

I could not help but walk out of Dr. Gu's talk hoping our government would proclaim a "moonshot" to reinvent our manufacturing infrastructure, lest the rest of the world ends up eating our lunch!

MILTON CHANG of Incubic Management was president of Newport and New Focus. He is currently director of mBio Diagnostics and Aurrion. He is a Trustee of the California Institute of Technology and has served on the SEC Advisory Committee on Small and Emerging Companies and the Visiting Committee on Advanced Technology of the National Institute of Standards and Technology, and the authoring committee of the National Academies' Optics and Photonics: Essential Technologies for Our Nation. Chang is a Fellow of IEEE, OSA, and LIA. Direct your business, management, and career questions to him at miltonchang@incubic.com, and check out his book Toward Entrepreneurship at www.miltonchang.com.